Spacecraft -Scale Magnetospheric Protection from Galactic Cosmic Radiation

Final Report

John Slough

MSNW LLC.

16436 SE 39th Place

Bellevue, WA 98008

Email: sloughj@msnwllc.com

September 2021

Summary

An optimal magnetic shielding configuration for significantly reducing astronaut exposure to Galactic Cosmic Radiation (GCR) on long interplanetary missions has been realized, and is referred to as the Magnetospheric Dipolar Torus (DTM). This configuration was shown to have the singular ability to deflect the vast majority of the GCR including High Z Energetic (HZE) ions. This external (to the spacecraft) dipolar field is created by an array of unidirectional toroidal High Temperature Superconductor (HTSC) windings mounted externally on the surface of the toroidally-shaped spacecraft habitat. In this way the spacecraft directly supports the magnetic hoop forces generated by the toroidal currents and thereby significantly reduces the structural mass requirements for the shield. The magnitude of the toroidal currents are arranged poloidally to flow so as to maintain the spacecraft shell as a constant flux boundary such that the magnetic flux $\varphi = 0$ inside the spacecraft keeping the habitat field-free with no need for providing additional coils to cancel the internal fields. As the dipole magnetic field is everywhere perpendicular to the spacecraft habitat, the DTM provides a deflecting shield to all the incoming GCR which is nearly isotropic. In addition, the DTM shields the HTSC coils as well thereby eliminating the secondary particle irradiation hazard, which can dominate over the primary GCR for shields with closed magnetic topologies. With DTM shielding it was found that both the structural and magnet mass as well as the total current requirements were significantly reduced. The DTM shielding effectiveness was calibrated in a large laboratory vacuum chamber experiment using a high energy beam as a surrogate for the GCR encountered in space. MSNW developed 3-D relativistic particle code to evaluate magnetic shielding of GCR and also employed a very accurate commercially available particle trajectory and magnetic field solver, Lorentz-3M, from Integrated Engineering to evaluate shielding effectiveness for the GCR spectrum encountered in space. The codes were employed to evaluate a wide range of magnetic topologies and shielding approaches including prior proposed magnetic shielding concepts. Four criteria for evaluation of the efficacy of magnetic shielding are discussed for three of the most developed concepts including the DTM. They are: (1) Effectiveness of the magnetic shielding using the level of protection achieved for a given magnetic geometry as a function of the magnet mass required. The DTM proved to be an order of magnitude better. (2) Issues with secondaries: The interaction of the GCR with large, exposed magnetic systems has a profound effect on the total radiation exposure inside the habitat independent of the shield effectiveness. (3) Launch and space assembly: The amount of mass, scale of structures, and complexity of assembly. (4) Advantages and other uses for the concept beyond GCR protection such as magneto-aerobraking and capture.

Table of Contents

1. Introduction **4**

2. Basic Analysis of Active Magnetic Shielding **4**

3. Past Efforts on Active Magnetic Shielding **6**

4. Dipolar Toroidal Magnetosphere (DTM) **8**

5. Comparison of prior proposed magnetic shielding geometries to the DTM **12**

6. Results from the Experimental Testing and Shielding Analysis of the DTM **30**

7. Summary **43**

8. References **44**

1. Introduction

It is well known that exposure to the ionizing radiation of galactic cosmic-rays (GCR) and solar energetic particles (SEP) is an important concern for the health of the crew for long duration interplanetary missions. [1-6] The question to be addressed here is whether or not it is feasible to mitigate this exposure in a practical manner. The SEP events are characterized by the emission of high fluxes of lower energy particles, which last on the order of hours to days (see Fig. 1). Although the intensity of the radiation is much greater than the GCR, passive shielding, i.e. shielding provided by the slowing down and absorption of the charged particles in inert materials, can be effective for SEP as the duration and penetration distance for these lower energy particles is quite short. The GCR flux however is near isotropic and is relatively constant, being modulated somewhat by the solar cycle. Periods of maximum solar activity result in the decrease of the low energy GCR flux due to their interaction with the higher particle flux emitted by the Sun. Previous analyses have pointed out the futility of attempting to employ a material barrier for the GCR as the increase in shield thickness creates a mass penalty that is far too great to be practical. Even partial shielding is not an effective option as the radiation hazard can actually be greatly enhanced in this case due to the "daughter" particles generated during the slowing down process of the GCR in the material. This is particularly true for the high charge and energy (HZE) ions such as iron which can create several high energy secondary and tertiary particles. The radiation risk arises from the damage caused by the energy lost from these charged particles in human tissue. The GCR fluxes represent a longer-term risk exposing the crew members to lower life expectancy due to radiation induced cancers.

2. Basic Analysis of Active Magnetic Shielding

Of all the active methods that have been suggested to take the place of passive (i.e. material) shielding, the most promising from a technological point of view, and the most studied, is the use of magnetic fields to deflect the GCR away from the human space habitat. The basis for this approach is given by the partial shielding provided by the Earth's magnetic field, however it is not Earth's magnetic field but rather the bulk of the Earth's atmosphere that protects us from the full brunt of the GCR. The physics behind the concept is simple and is based on the fact that a charged particle in traversing a transverse magnetic field will experience a transverse acceleration to its direction of motion due to the Lorentz force:

$$\vec{F} = q\vec{v} \times \vec{B} \qquad (1)$$

As this is a non-central force, the kinetic energy of the particle is undiminished and is not reduced by this interaction. Only the direction of motion can be changed. In a uniform, transverse

(to the particle motion) magnetic field **B** the particle executes a circular motion at a radius r_L (Larmor radius) given by:

$$r_L = \frac{mv_\perp}{qB} \cong \frac{mc}{qB}, \qquad (2)$$

where it is recognized that these high energy (~ GeV/nucleon) particles will be moving close to the speed of light so that m represents the relativistic particle mass. In order for a magnetic field to deflect a charged particle in a variable magnetic field, such as occurs in a magnetospheric dipole field, the integral of the magnetic field over the path of the particle motion within the magnetic shield must be sufficiently large (i.e. comparable to the gyro-radius of the particle) or,

$$v_\perp \simeq \frac{q}{m}\int B_\perp dr \qquad (3)$$

where q is the charge of the particle, and the subscript ⊥ denotes quantities perpendicular to the magnetic field. Any particle with $v_\perp$ less than the value found from Eq. (3) will be deflected, irrespective of its initial pitch angle. For shielding of MeV protons and 1 GeV electrons, Eq. (3) then requires that $\int \boldsymbol{B}_\perp dr$ be of the order of 0.1 Tesla-meter (T-m). Deflection of a GeV proton would then require $\int \boldsymbol{B}_\perp dr$ to be of the order of 3 T-m while solar wind particles would only require 0.001 T-m. This criterion is a necessary condition but it turns out to not be a sufficient condition. Magnetic shielding must be verified by single particle tracking techniques like those that were developed in this study, and similar to the Monte Carlo techniques developed elsewhere for this purpose. [7,8]

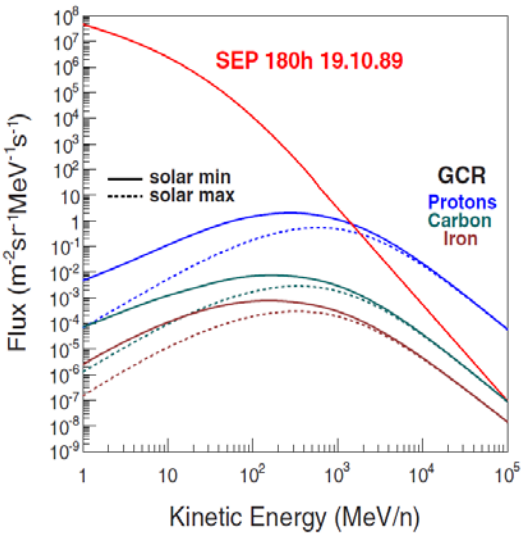

Figure 1. The proton flux of a 10-day SEP event in 1989, and the GCR proton, carbon, and iron nuclei fluxes for solar minimum and maximum periods (From Ref. 2).

For scaling purposes though the simple deflection picture is adequate. In a spatially uniform magnetic field, the distance L the particle must travel transverse to this B field to be deflected by an angle θ is given roughly by:

$$\theta = 2\sin^{-1}\left(\frac{2L}{r_L}\right) = 2\sin^{-1}\left(\frac{2}{c}\frac{q}{m}BL\right). \qquad (4)$$

Clearly one wishes to maximize B and L. The other key variable is the charge to mass ratio q/m. This is where active magnetic deflection has a great advantage over passive shielding. This

ratio is roughly constant at ~ 0.5 coulomb/nucleon as one goes from helium to iron. While hydrogen has a somewhat more favorable ratio (unity), the magnetic field deflection of HZE ions like iron will be as effective as that for deflecting lighter ions with the same charge to mass ratio. This of course is with the caveat that these HZE ions do not encounter material objects. In that case the tissue damage from the subsequent particle cascade can more than make up for their much lower GCR population.

3. Past Efforts on Active Magnetic Shielding

There have been several groups that have presented active shield designs based on superconducting magnet configurations. Virtually all have assumed shield configurations composed of toroidal or solenoidal magnets. There is a very good reason for this. With the advent of High-Temperature SuperConductors (HTSC), it is possible to achieve very high magnetic flux densities at operating temperatures (~25 -75 °K) that do not require the use of liquid helium thereby alleviating the technical difficulties in providing for the stability of a cryogenic system in space. There have been two main studies employing HTSC shields that employ B field coils partially surrounding the spacecraft habitat with the high magnetic fields concentrated in a layer radially outward from the habitat (see Fig. 2). These were performed by the European Space Agency which employed a toroidal magnetic geometry (ESA toroid) [9], and The NASA NIAC study [4] which employed a circular array of 6 large solenoidal coils with a central seventh coil operated in the

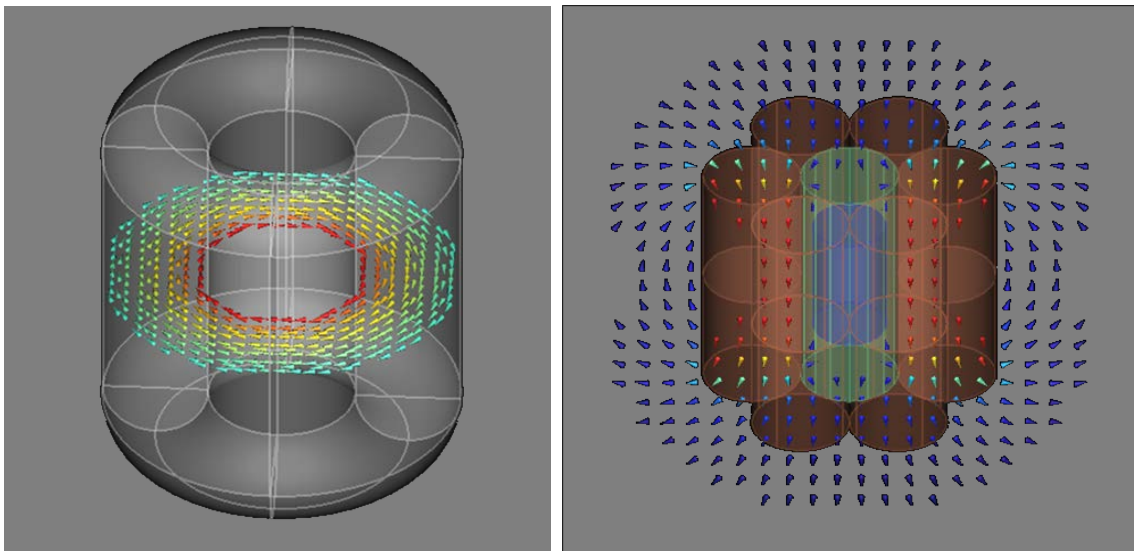

Figure 2. 2D magnetic vector plots for (Left) ESA toroid at midplane, and (Right) 6-1 solenoids. The vectors are color coded red to blue indicating magnitude of the field. The plots range from the maximum field down to 5% of the maximum. The ESA toroid had no external fields larger than 1% of the maximum outside of the torus.

reverse sense to buck out the magnetic field created by the six surrounding solenoids (NASA 6-1 solenoids). The idea being in both cases that a high B·L product can be achieved at least for GCR flux coming in the radial direction toward the habitat.

The HTSC shields for the studies were as follows: Yttrium-Barium-Copper-Oxide (YBCO) for the NASA 6-1 Solenoids and Magnesium Diboride (MgB_2) for the ESA Toroid. The performance of these designs was evaluated based on the results obtained with 3-dimensional Monte Carlo simulations that propagate the charged particles in the magnet field, and generate interactions of the particles in the materials of the coils and support structures of the magnet shield. Even with extrapolations of existing technology for the materials of the coils and support structures of the magnet shield, the results were not encouraging. The results from the calculation can be found in Fig. 3 taken from Ref. [1]. The performance is expressed in terms of the contribution of the field to the overall dose reduction of the shield, including the passive shielding elements, and the combined shield plus habitat dose level with respect to the habitat dose level. As can be seen, the role that the magnetic field plays in reducing the primary GCR is significant but the total effect on radiation exposure is paltry at best. The NASA 6-1 Solenoids numbers are within error bars of having no net effect at all. It should be noted that the GCR that come from the polar regions (see Fig. 2) were not considered, so even the magnetic shielding reduction in Fig. 3 does not reflect

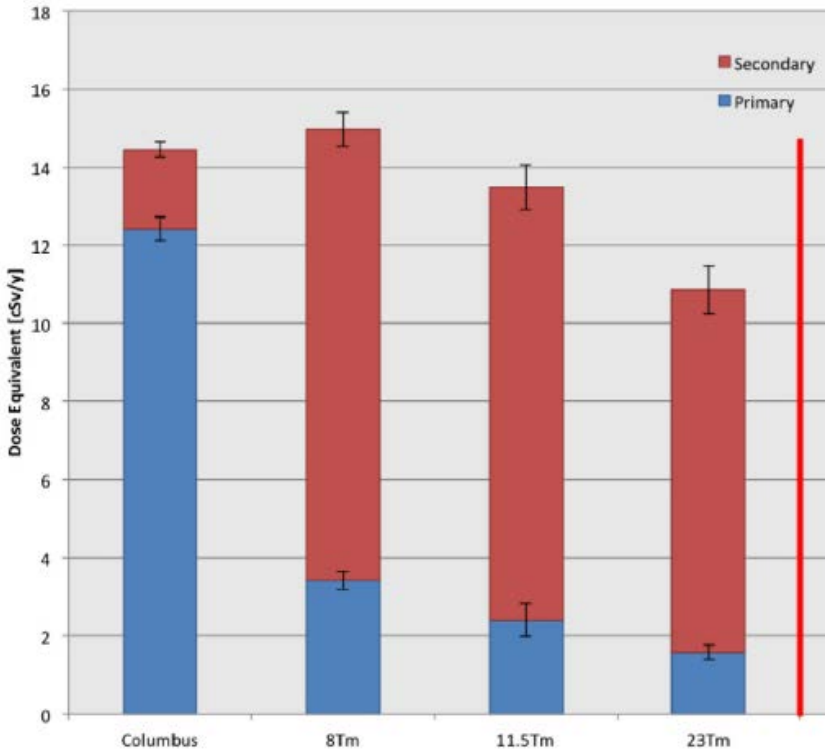

Figure 3. The contributions of the primary GCR proton and He nuclei, and the secondaries produced in the material of the ESA Toroid habitat (Columbus) and magnet for various BL products (in T-m) up the limit of HTSC technology indicated by the red line.

these marginally deflected particles.

The lack of efficacy stems from the magnetic topology of the approaches taken in these concepts. It is clear from equation (3) that to deflect the GCR particle, the magnetic field must be perpendicular to the direction of motion. Since particles can come from any direction, deflecting only those coming in perpendicular to the primarily axial or azimuthal B field will suffice. This "hole" on-axis allows primary GCR to enter unabated. In fact, some GCR particles can be deflected into this region by the very fields meant to keep them out. The results from the GCR particle tracing to be discussed later clearly illustrate this vulnerability, particularly for the ESA toroid. The radiation protection with regard to these "closed" magnetic field configurations is made worse beyond the lack of adequate coverage. A major problem is the lack of any significant magnetic shielding for the coils themselves as these are exposed to the GCR flux also unabated. The cure now becomes the disease as the coils become the passive source of a cascade of daughter particles. This is the reason for the lack of total radiation reduction in Fig. 3. The reduction in primary GCR ions due to the shield is more than made up for by secondary emission for all but the highest B·L product technologically feasible at this time with HTSC magnets.

4. Dipolar Toroidal Magnetosphere (DTM) Shielding

It can be readily argued for active magnetic shielding to be a viable option, that at a minimum the following criteria must be met: (1) The magnetic shield must deflect the vast majority of GCR ions including HZE ions. (2) The magnets must not create additional high energy particles from passive absorption. (3) The structural, mass, and power requirements for the shield must not

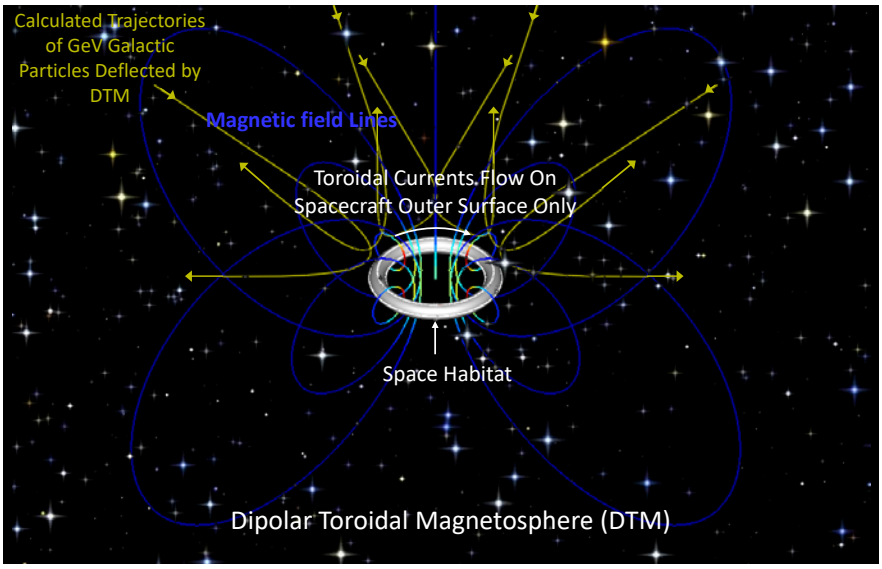

Figure 4. Dipolar magnetospheric shielding provided by toroidal currents I_c. The HTSC magnet (sliver colored shell) is placed external to the toroidally shaped space habitat. The magnet would fully surround the habitat to assure cancelation of all magnetic field inside the habitat.

become “the tail that wags the dog”. (4) The shield development roadmap must allow for both analytical and experimental validation at much reduced cost and scale prior to full deployment.

It is believed that all four of these criteria can be met by the shielding concept described in this section. It is also believed that the magnetospheric approach taken here is likely to be the only one that can. There are very good reasons for that belief based on the physics and topology requirements for an effective shield. To understand why previous conceptual designs have failed to satisfy these criteria, and how the proposed approach avoids these pitfalls, a brief discussion will be given that illustrate the key principles that must guide the design of an effective magnetic shield. Adequate shielding in all directions, as well as protection of the magnets themselves can be accomplished by employing a Dipolar Toroidal Magnetic (DTM) field, where the habitat takes on the form of the shielding magnets as depicted in Fig. 4. In this way the spacecraft can directly support the magnetic hoop forces generated by the toroidal currents and thereby significantly reduce the structural mass requirements for the shield. It should be noted that the dipole currents all flow around the toroid in a shell surrounding the habitat, but in the same *toroidal* direction. In the ESA studies the coils also have a toroidal geometry. In this case however, the currents flow only in the poloidal direction, as is typical for a conventional toroidal magnet, thereby creating a

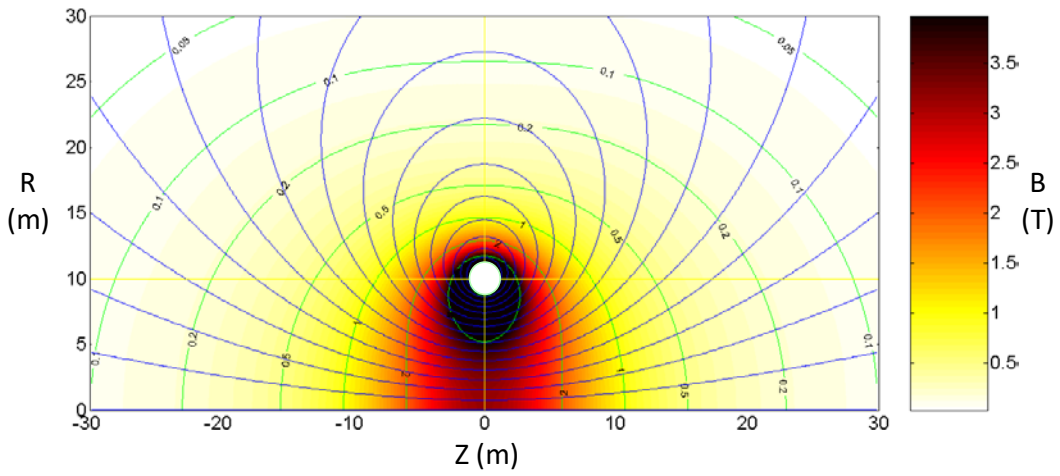

Figure 5. Flux lines and magnetic contours for a dipole torus. Here the current flows only at the toroid surface such that the magnetic field vanishingly small inside.

toroidal field only on the inside of the toroid. This region is thus inhabitable and the structures required to support the coils adds considerable additional mass. This same shortcoming can be found in the NASA 6-1 Solenoids where an array of six, long solenoidal magnets surrounded the spacecraft and required an additional coil to buck out the return flux from these coils from the spacecraft habitat which diminishes the effective shielding. More will be said of these two concepts in the nest section as they comprise the leading alternative magnetic shield concepts prior to this study.

In contrast, the external dipolar field created by the unidirectional toroidal currents in the shell all add to the strength of the external dipole field outside the space habitat. In this scenario, there is no need for providing additional coils to cancel the internal fields as in the other approaches. The toroidal currents are arranged to flow so as to maintain the shell as a constant flux boundary

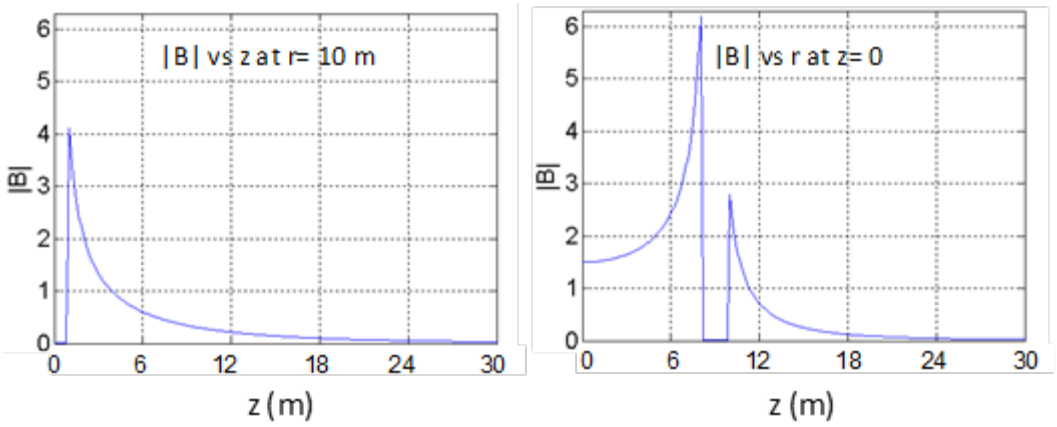

Figure 6. Modulus B as a function of z on axis and at the major torus radius R = 10.

where the poloidal flux $\varphi = 0$. It is easiest to see how this can be arranged by considering a cylindrical tube carrying a uniform axial current along its length. The B field created is purely azimuthal (i.e. poloidal) and vanishes inside the wall of the cylindrical conductor, which can be easily confirmed by a simple application of Ampere's law at any radius inside the cylinder. Bend this cylindrical tube into a torus and you have the situation desired here. The toroidal currents in this case however do not flow at a constant magnitude at all azimuthal angles around shell periphery as it does for the cylinder. Only for torii at very large aspect ratio (torus diameter/habitat diameter $\equiv \alpha$) does it approach uniformity. For a typical aspect ratio $\alpha \sim 10$, a larger current must flow on the inner wall of the torus to maintain the $\varphi = 0$ state inside the habitat (see Figs. 5 and 6).

Analysis of the shielding for this dipole torus was conducted with a particle tracing code developed at MSNW. The magnetic field and flux for a realistic scale dipole torus is shown in Fig. 5. The magnetic field strength is characterized by the magnetic field B_{00} at r = z =0. Plots of the magnetic field on axis and at r = 10 m as a function of is shown in Fig. 6 which clearly show how the field (and thus I_ϕ) is significantly higher on the inboard side of the torus for a toroid with an $\alpha \sim 10$ as is the case here. The characteristic axial field strength on axis at the center of the toroid, B_{00} = 1.5 T for this case. The effectiveness of the magnetospheric dipole in deflecting GeV GCR particles can be seen in Fig. 7 where it was found to be sufficient to exclude all particles from a significant volume about the dipole. This is clearly where one would place both the space habitat and toroidal coils providing full protection from GCR bombardment.

From both a confinement and shielding perspective, as well as the obvious choice for simplicity, shielding from an array of geometrically simple circular loops of conductors as proposed here was

found to be the most favorable. A code to calculate the particle motion in a 3-D magnetic field was developed and tested, and was found to be quite accurate. It is possible however to do some analytic estimates that reproduce with reasonable accuracy the results from the 3-D numerical calculations. Since it is easy to calculate the field from a single loop (or sets of loops as in the toroidal shield), the shielding effectiveness can be characterized by the B_z field on axis at the center of the toroid (B_{00}), and the far-field dipole magnetic field $B_z(r)$,

$$B_{00} = \frac{\mu_0 I}{2R} \quad \text{and} \quad B_z(r) = gB_{00}\frac{R^3}{r^3}, \tag{5}$$

where it was found that g = 0.5. B_{00} is typically less than the field strength at the torus boundary but serves the purpose of relating the field strength to the shielding effectiveness. If one assumes that an incoming particle penetration distance must be less than a characteristic deflection distance (see Eq. 4), one has

$$\int_{l_1}^{l_2}\frac{dl}{r_L} \geq 1 \quad \rightarrow \quad \int_{r_0}^{\infty} B\cdot dr \geq \frac{m}{q}\gamma v \tag{6}$$

where the relativistic nature of the GCR particle is explicitly expressed. Integrating using Eq. (5) one obtains:

$$B_{00} \geq \frac{m}{q}\frac{4\gamma v r_0^2}{R^3} \sim \frac{m}{q}\frac{4\gamma v}{R} \tag{7}$$

Where the approximation assumes that smallest characteristic deflection radius r_0 is assumed to be roughly that of the torus radius R. For a 1 GeV proton one has $\gamma v = 5.4\times10^8$ m/s. For a loop radius of 10 m one has $B_{00} \geq 2.2$ T. This turns out to be somewhat more restrictive than the detailed

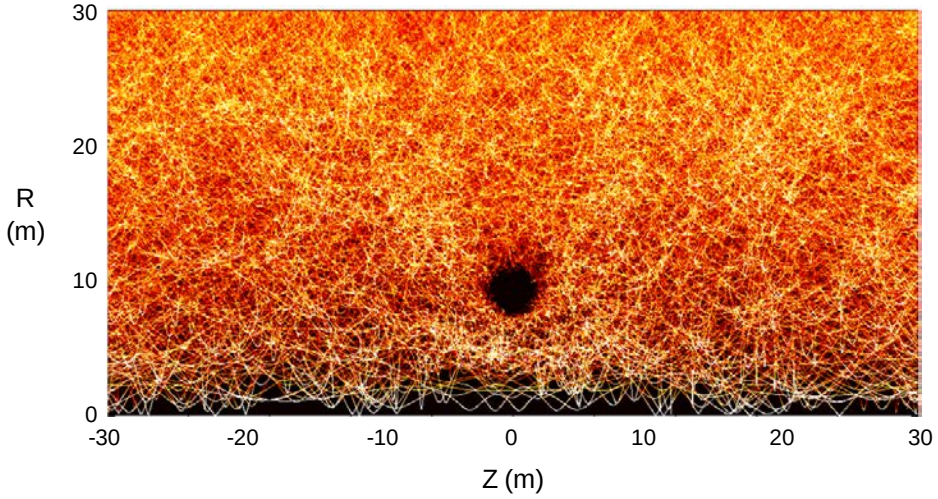

Figure 7. Trajectories of 1500 isotropic 1 GeV particles on to dipole ring. Apparent shielding at small r only reflects the volume reduction as r ⇒ 0.

particle calculations, but close enough for most purposes such as scaling, current, and structural requirements. The results from the particle calculations for the Dipolar Toroidal Magnetosphere (DTM) with $\alpha = 10$ are shown in Fig. 7. It can be seen that complete shielding can be obtained for higher energy nucleons by increasing the magnetic field and that partial shielding is possible even at higher energies although the effectiveness diminishes for these higher energy GCR particles.

5. Comparison of prior proposed magnetic shielding geometries to the DTM

Several different magnetic configurations were evaluated taking into consideration both feasibility and simplicity. For "open" systems where the magnetic field is not primarily confined by a conducting boundary, the best candidate is the magnetic dipole as it has the slowest falloff with distance ($B \sim 1/r^3$). For a closed magnetic geometry, there appear to be two well researched and characterized candidates, the NASA 6-1 solenoids and the ESA toroid discussed earlier. These two will now be characterized using a commercial 3D code, Lorentz-M® that can accurately calculate the magnetic fields from any specified array of current elements, as well as track the relativistic trajectory of emitted particles in these fields. By using this code, an unbiased and accurate comparison of the relative effectiveness of the proposed shield concepts was made.

Just as important as the calculation accuracy is a method for normalizing the results across all three concepts, so that a valid comparison can be made as the total current requirements, magnetic field strengths, and magnet mass are all different for each model. It will be argued that the normalization criteria should be the total HTSC mass required for a given GCR reduction normalized to the habitat volume, V_{hab}. The additional mass required in space to protect a given spacecraft habitable volume is clearly a "bottom line. As different concepts considered different types of High Temperature Superconductor (HTSC), and at different current densities, a better metric is the total current required, I_{tot} times the conductor length required,$\cdot L_c$. This quantity is independent of the type of HTSC and assumed maximum current density J_{cr}. It is however directly proportional to magnet mass. Once the optimal HTSC and its maximum current density has been determined it should be the same for all concepts. This key ratio of $I_{tot} \cdot L_c / V_{hab} \equiv \Omega$ then is the primary criterium in evaluation of the effectiveness of shield. Another important element is the maximum magnetic field stress felt by the magnet structural system. This is harder to normalize due to the different habitat configuration geometries. It should however be a part of the criteria in a general way as the structural magnet mass requirement will be driven by the maximum surface area, A_s, exposed to the magnetic field as the force on the structure scales as $B_s^2 \cdot A_s$.

There are several other elements that could favor one approach over another such as the ease of assembly of the structures and coils required in space. The ability to launch subassemblies for easy assembly is clearly a plus. A critical consideration is whether the magnet system itself poses additional radiation concerns due to daughter particle generation from GCR striking the large magnet structures. As mentioned, previous analysis of the "closed-field" concepts indicate that this turns out to be a very significant problem for as there is very little, if any, deflection of GCR

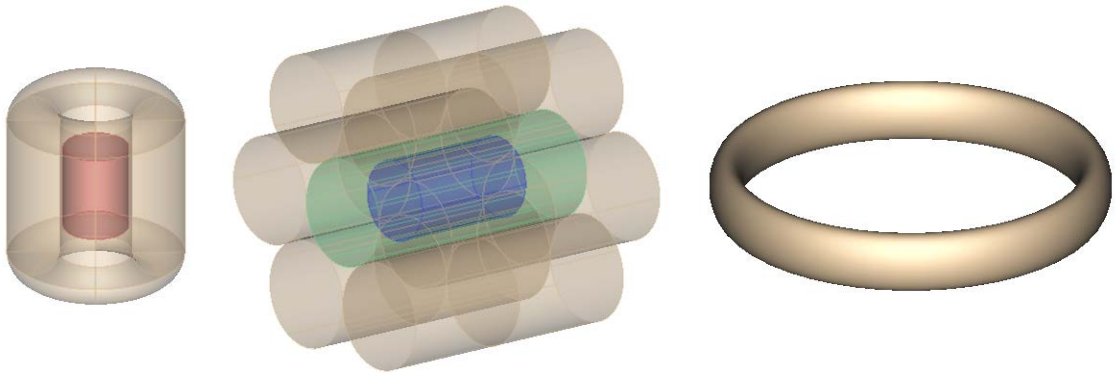

Figure 8. Magnetic coil surfaces and habitats assumed in the ESA-T, N6-1 Sol, and DTM studies. Left: ESA-toroid (length – 13.6 m, width at midplane – 3.6 m, bore – 3 m) with Columbus habitat inside (4.5 m diameter, 6 m long). Center: NASA 6-1 solenoids with 6 outer solenoids with inner solenoid carrying reverse current (8 m diameter, 20 m length). Cylindrical habitat is 3 m diameter and 10 m in length. Right: DTM with a toroid major radius of 12 m and a 4 m by 2.2 m elliptical cross-section. As the current coils are supported by the spacecraft habitat wall, the coil surface and habitat cannot be distinguished

external to the magnet. With the coils placed in a manner that engulfs the habitat along with the fact that the extent of the coils being considerably larger than the habitat itself, creates a much larger source for this particle-cascading process and it occurs prior to any significant reduction in GCR flux.

Finally, does the magnetic deflection scheme employed for optimal shielding effectiveness (e.g. the toroidal geometry of the DTM) provide for additional benefits in terms of human health. With a large aspect ratio toroidal habitat, the possibility of an artificial gravity can be readily achieved through simple rotation of the torus in the toroidal direction. Evidence from spaceflight and spaceflight analogs such as the NASA Human Research Exploration Analog (HERA) suggests that the Risk of Adverse Cognitive and Behavioral Conditions and Psychiatric Disorders (BMed) poses a high likelihood and high consequence risk for extended and planetary exploration [10]. Given the possible synergistic effects of prolonged isolation and confinement, radiation exposure, and prolonged weightlessness, mitigating such enhanced risks faced by future crews are of highest priority. It is likely that isolation and confinement can only be resolved by shorter trip times [11]. The radiation exposure and prolonged weightless can be simultaneously resolved by implementation of the DTM. In summary then, one can derive four main criteria which will be

used to evaluate the three most developed concepts those being the ESA Toroid, the NASA 6-1 Solenoids and the DTM. They are:

(1) Effectiveness of the magnetic shielding – This will be determined using the Ω parameter defined above as it is the best measure of the protection realized for a given habitat and magnetic geometry as a function of the magnet mass required.

(2) Issues with secondaries - The interaction of the magnetic structural topology for each concept can have a significant effect on the type of radiation exposure experienced inside the habitat from the structures themselves regardless of the effectiveness of the magnetic deflection from the magnet.

(3) Launch and space assembly – The amount of mass, scale of structures, and complexity of assembly of the magnet systems must be characterized as the cost of access to space is still and determining factor in concept feasibility.

(4) Advantages and other uses for the shield outside GCR protection. Given the likely high cost of the shielding systems, what other uses for the shield might there be besides crew protection that would help justify the investment in the shield deployment.

These four criteria for concept evaluation will now be discussed in turn for the three proposed concepts.

Criterion (1): Effectiveness of the magnetic shielding

The characterization of the shielding concepts represented by the ESA toroid, the NIAC 6-1 solenoids, along with the DTM will now be described in more detail. Figure 8 illustrates the magnetic coil (current) surfaces and habitat assumed by the various concepts. These and formed the basis for the input into the Lorentz 3M calculation carried out identically on all three concepts. As was mentioned the analysis of the efficacy is measured by the total HTSC mass per unit volume of habitat, or

$$\Omega = \frac{\sum_{1}^{n} I_n \cdot L_n}{Vol_{Hab}}, \qquad (8)$$

where the sum is over all the current elements times the length of that current element, and Vol_{Hab} is the total volume of spacecraft habitat protected by the magnetic shield. The sum will be proportional to the total mass of the HTSC coil system and has the advantage that it does not specify what HTSC is employed. In previous studies the assumed HTSC was folded in to both the mass calculation as well as the size of the field generated, which made comparisons difficult. Here it is assumed that the optimal HTSC for shielding should be independent of the magnetic system employed, and avoids a down-select until the optimal configuration has been determined based on Ω.

It should be noted that the habitat size, shape and volume are not independent variables. Variations in scale for a given topology will reflect different Ω's. Generally speaking, the larger the habitat, the less Ω is required. There is no easy way to normalize the habitat for all three

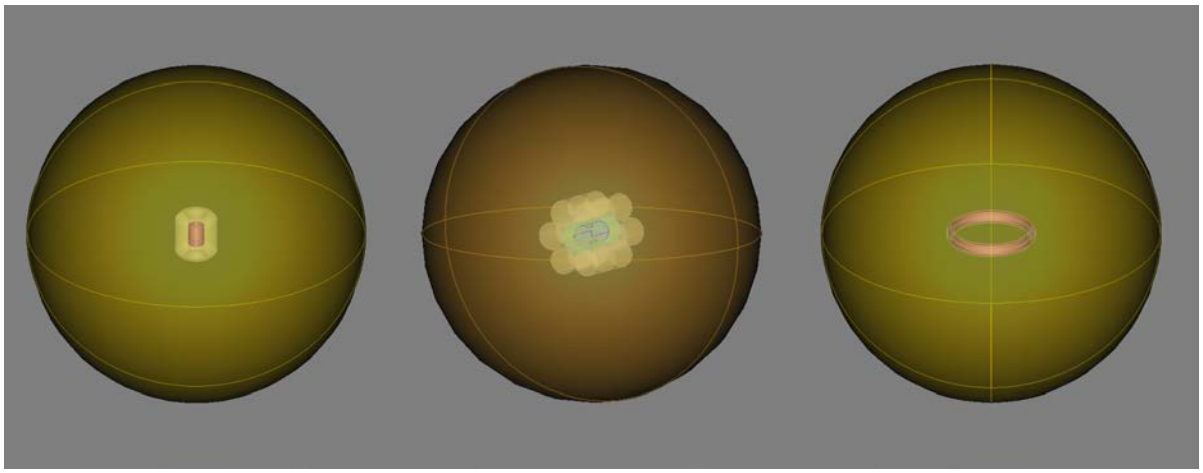

Figure 9. Spherical surfaces for the random launch of GCR test particles for isotropic bombardment of the three magnetic shield configurations. The magnetic coils are shown as semi-transparent with the habitat incased within as described for the three concepts. The meridian lines are for showing position of spherical surface and had no significance with regard to the calculations.

concepts, and using the actual habitat geometry and size proposed was the next best option. Doing so allowed for the extensive Geant 4 radiation calculations [1] performed on these concepts to be used in helping to assess issues in regards to secondaries (see criteria 2 above).

There was also no reason to use the entire GCR spectrum in evaluating the three concepts as the principle means of protection (magnetic deflection) is more easily observed under simpler, but an equally accurate assumption for comparison purposes. Given the seasonal variation in GCR exposure as well as the essentially untested dependence of radiation risk on GCR energy, it was decided not to fold these considerations into the comparison. That is not to say these considerations are not important, but again it is something to consider after choosing the best magnetic shield configuration in deflecting any GCR. It was thus decided to carry out the comparison for deflection of the GCR at the peak of the GCR radiation power curve, and for the largest contributor at that energy. In other words, an isotropic emittance of 500 MeV protons was used to test the three concepts.

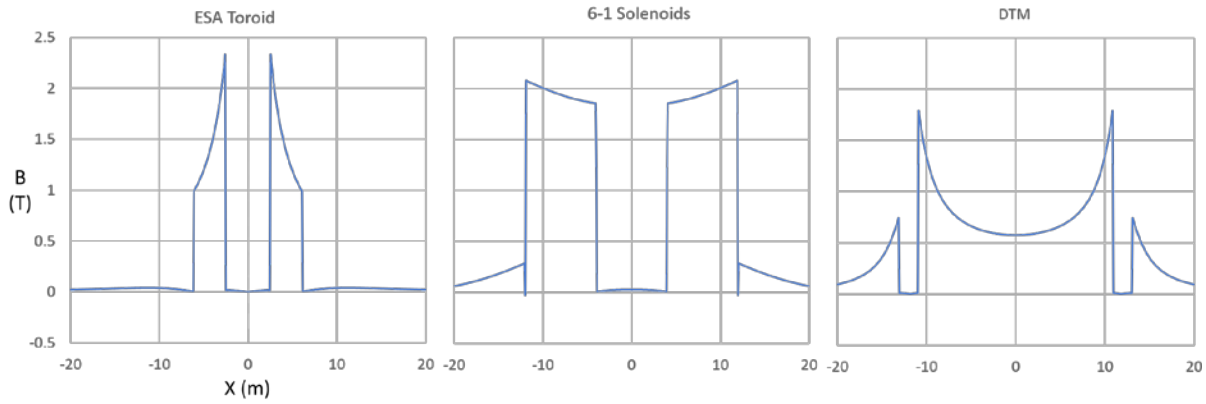

Figure 10. Magnitude of the magnetic field for the three concepts shown in Fig. 8 along the X-axis. The X-axis was chosen to lie in the plane of mirror symmetry for each configuration and along the direction that was perpendicular to the magnetic field direction thereby reflecting the maximum magnetic field strength. This X-axis can be chosen to be in any direction in this plane for the ESA Toroid and the DTM due to azimuthal symmetry. It was oriented to pass through the central axis (Z-axis) of three of the 6-1 Solenoids (two outer and the one central).

The 500 MeV protons were launched from the surface of a sphere with a 100 m diameter for all three cases. The large standoff was necessitated by the deflection from the external field of the DTM was still evident at large distances from the toroidal dipole coils. The difference in deflection effectiveness was becoming small enough at a launch radius of 50 m that it made only slight differences (< 5%) compared to 100 m. The smaller launch radius of 50 m was still much greater than used in previous calculations for the ESA and NASA concepts. The GCR source sphere in

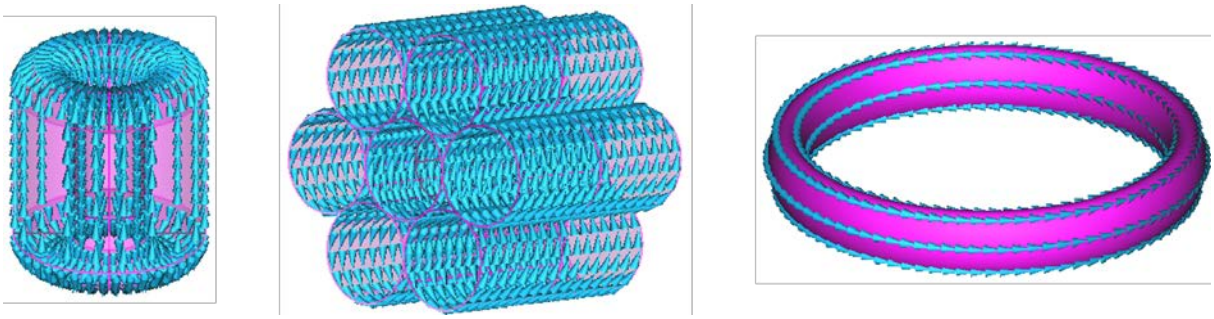

Figure 11. Direction of current flow for the three concepts. All currents are surface currents. The magnitude of the current is uniform around the toroidal direction for the ESA toroid, but varies in the poloidal direction as the surface cross-section changes from inside to outside. The azimuthal currents in the 6-1 solenoids are also uniform along the Z-axis for each solenoid, and is equal in magnitude for the outer six solenoids. The toroidal belt currents in the DTM vary in strength poloidally from the inner side to the outer side so as to maintain the magnetic flux inside the ellipsoidal toroid near zero, i.e. a null magnetic field (see Figs. 6 and 8).

relation to the three coil systems and habitats can be found in Fig. 9. Over twenty thousand protons were launched at random angles. The angular spread was governed by a cosine distribution to the normal at any given point on the sphere to avoid launches far from the target direction in order to keep the calculation time reasonable. With the magnetic field turned off, roughly two thousand, 500 MeV protons struck and were collected on the habitat surface. The total current in the coils was then increased until 75% of these protons were deflected sufficiently so that they failed to

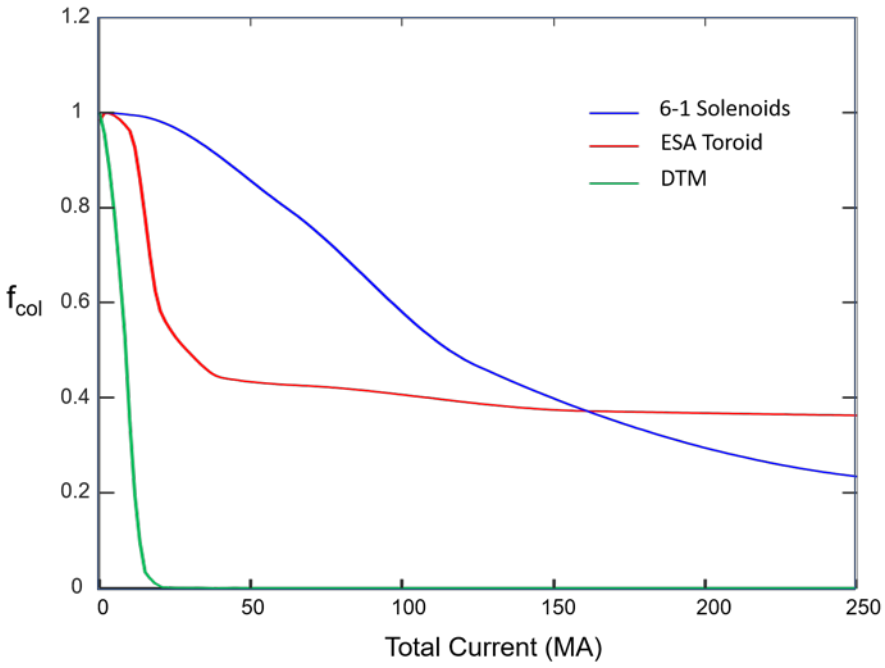

Figure 12. Fraction of 500 MeV protons reaching the habitat of the various concepts as a function of the total current.

reach the habitat surface and were terminated back on the spherical boundary.

A plot of the magnetic field profiles required to obtain this level of shielding is shown in Fig. 10. It is clear from this figure that the DTM requires less field for the equivalent GCR deflection effectiveness. A significant contributor to this superiority is due to the larger scale of the current loops employed to generate the field as this in turn provides for a larger scale length to the external magnetic field that does the deflecting. A plot of the current flow for the three concepts is shown in Fig. 11 illustrating the point.

The measure of shielding efficiency, Ω, between the concepts was more notable. The Ω value for the three cases at 75% primary proton deflection was: Ω = 55 MA-m^{-2} (ESA Toroid) = 22 MA-m^{-2} (6-1 Solenoids) = 1.7 MA-m^{-2} (DTM). The DTM was found to be over an order of magnitude better at shielding per unit habitat volume than the other two concepts. Plots of the fraction of

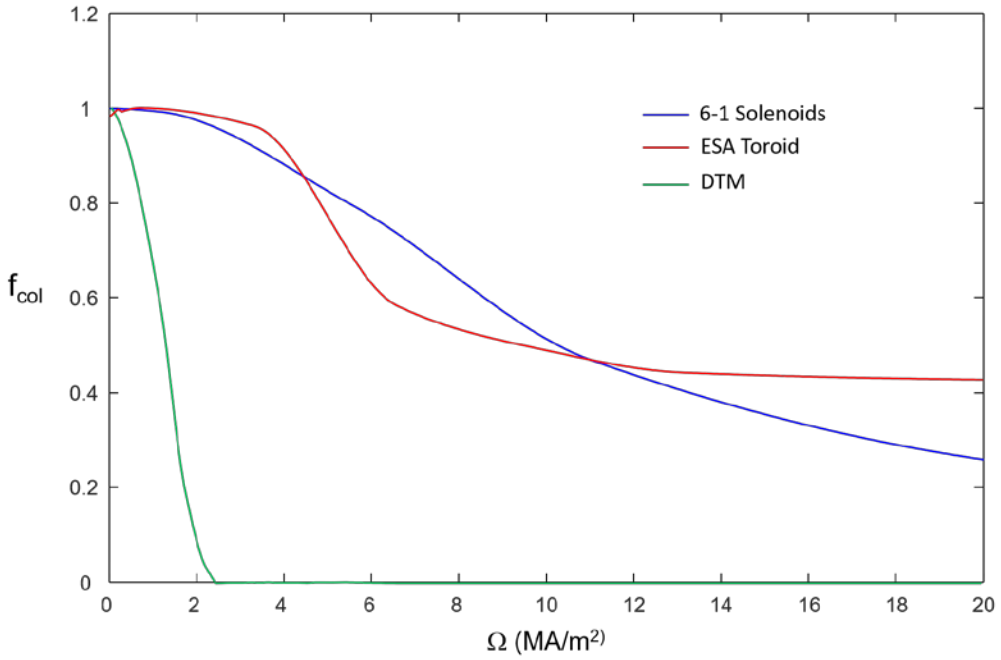

Figure 13. Fraction of 500 MeV protons reaching the habitat of the various concepts as a function of the efficiency parameter Ω.

protons striking the habitat as a function of total current and Ω can be found in Figs. 12 and 13. There are several reasons for this. As mentioned, the current loop for the DTM is large and while it is the product of the current times the loop length that determines the magnet mass, the much larger scale of the magnetic field generated more than makes up for this. For the ESA toroid case, there are two reasons that the results were more unfavorable for this magnetic configuration. The biggest problem was the lack of protection for GCR that can enter through the end regions at the toroid hole. The magnetic field is contained only inside the toroid which

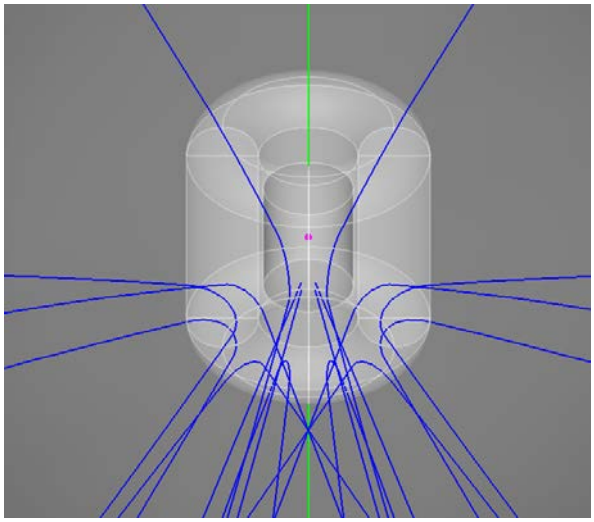

Figure 14. Selected proton trajectories from polar region of GCR sphere for ESA toroid.

leaves these regions completely exposed. The axial entry is also an issue for the 6-1 solenoid. The primary deflection is only for GCR particles that enter the coils in the direction perpendicular to the axis of the coil magnetic fields. The NASA 6-1 solenoids case is not as bad as the ESA toroid because the solenoids are essentially very elongated dipoles and the return flux from the coils' interior region is not cancelled by the reverse coil so that there is some external field protection in the end region from the return flux (see Fig. 2).

Thus, neither configuration can provide anything close to full shielding at any GCR energy. This vulnerability of the ESA toroid is quite evident in Fig. 14. The toroid is a good deflector of GCR coming more or less radially from what was referred to as the "barrel region". After a precipitous drop in penetration from these protons the level of protection plateaus around 40 % of the unshielded case, and increases in coil current have only a marginal effect. This is simply due to essentially no magnetic protection over a wide solid angle at each end. Trajectories of a small random sample of the 500 MeV protons launched form the lower end (polar) region of the GCR launch sphere that interacted with the ESA toroid fields is shown in Fig. 14. The particles that intercept the toroid are deflected while those that enter the toroidal hole where the habitat is located end up terminating on the habitat. The magnetic field vector plots shown in Fig. 14 illustrates this problem. The NASA 6-1 solenoids had some capability to provide protection to GCR from the polar region. Since the external fringe fields form the solenoid are weak, only extremely large currents could suppress the particles launched from these polar regions.

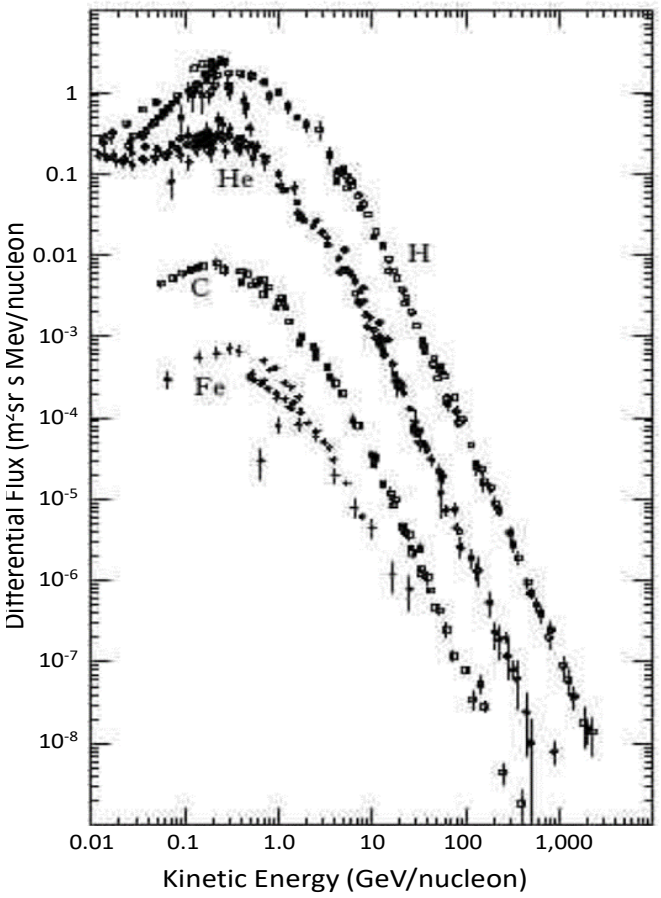

Figure 15. GCR flux for the most prominent GCR particle as a function of their kinetic energy, E_k.

The answer as to criterium (1) then is that the DTM is considerably more efficient in providing GCR shielding, and has the capability to completely extinguish GCR up to an energy determined only by the strength of the magnetic fields. The total effectiveness of the DTM over the entire GCR spectrum, as well as target values of current and Ω values for a significant reduction in total GCR exposure will be discussed in more detail later after a discussion of the experimental results

in the next section. It turned out that these results led to an improved DTM shielding design that wasn't obvious from the particle deflection calculations performed for the concept comparisons. It pertains to the assumption made in past numerical work that the shielding currents were comprised of continuous current sheets for the generation of the magnetic fields. This was a useful simplification for code calculations, but as will be shown, discrete conductors can be more effective if an array of cable bundles is employed in an optimal way. This was pursued first in the experimental testing as at that time the code work had not evolved to the point where discrete volume carrying conductors of arbitrary shape had been considered. The experimental setup and testing will be presented for the DTM after completion of the criteria evaluation

***C**riterion (2): Issues with Secondaries*

As indicated earlier, the interaction of the GCR and the magnetic structural topology for each concept has a significant effect on the type of radiation exposure experienced inside the habitat from the structures themselves. Given the many orders of magnitude over which the energy that

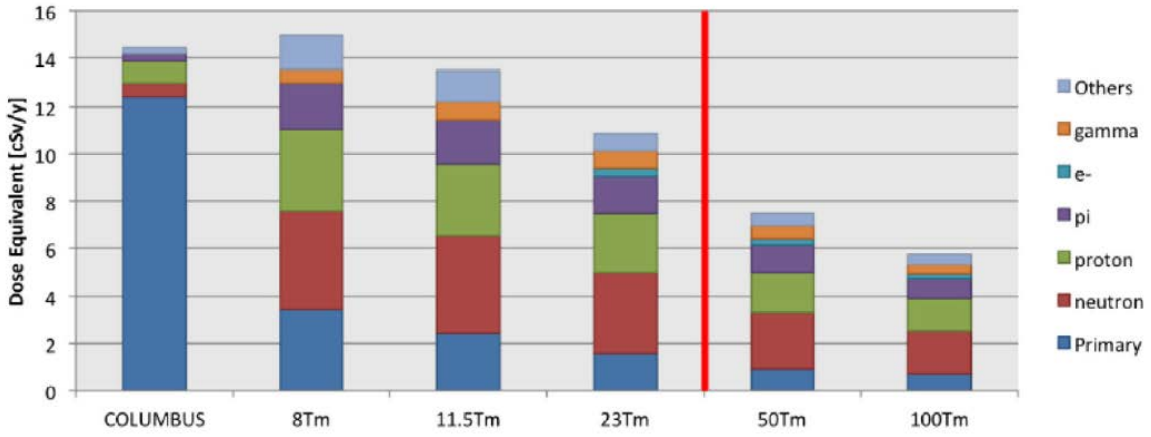

Figure 16. The annual body dose equivalent of the primary GCR proton and He nuclei, with a breakdown of the contribution of each of the principal secondary particles. The 50 and 100 T-m configurations require field flux densities that exceed the performance of present-day HTSC. (From Ref. [1])

the GCR is observed (see Fig. 15), there will always be some GCR with energies beyond any type of shielding and penetrate into the magnetic structures, as well as the spacecraft itself. Thus, all three concepts considered in section III will be vulnerable at some level to daughter particle production. While it is true that all are vulnerable, what is critical here, is the degree to which they are vulnerable. As pointed out earlier, neither the ESA toroid nor the 6-1 solenoids have significant magnetic field in the spaceward direction, so that these systems are essentially vulnerable to *all* GCR – even the lower energy ones that are deflected by the internal (to the magnet) magnetic fields created by these magnetic structures. It is not surprising then that secondary high energy particles are of major concern for these concepts. This is borne out by the data shown in Fig. 5

taken Ref. [1]. Clearly, by deflecting the vast majority of GCR prior to reaching the magnets and/or habitat as is the case for the DTM, the problem of secondaries is considerably mitigated. The results from the Geant 3 and 4 calculations show that the situation can actually be made worse due to the interaction with the magnetic structures. There are several reasons for this. As mentioned, the magnetic shields are exposed in much the same way as the unprotected spacecraft would be without them. The spatial scale of the shields is much larger than the actual habitat so that the number of intercepted GCR is much greater than had the shields not been present. Finally, the daughter particles include new types of radiation such as gamma rays and neutrons that cannot be ameliorated by magnetic deflection. A breakdown of the various components of the radiation field with and without the shields can be found in Fig. 16 taken from Ref. [1]. It is worth pointing out a few interesting results that this figure makes apparent. The magnetic field significantly reduced exposure to primaries with the initial application. The decrease in primaries is then only slowly reduced as the field is significantly increased as was seen in the particle trajectory analysis shown in Figs. 12 and 13.

The baseline flattening observed in the calculations for the ESA Toroid showed a plateau at a much higher value than Fig. 16 due to the inability of the Toroid fields to block polar GCR. The reason for the improved performance shown in Fig. 16 was that these end-on GCR were not even considered in the calculations for Fig. 16. Only GCR coming from the "barrel" region of space were considered. The primary driver to higher magnetic fields was the need to reduce the secondaries, at least the small amount that can be influenced with magnetic field deflection, as that appeared to be the only way to get the net exposure to less than the spacecraft with no shielding at all (the first column in Fig. 16).

While it is very likely that there will be no secondary issue for the DTM, particularly with discrete cables of HTSC current carriers, it is left to future work to apply the Geant 4 code and provide a definitive measure of the reduction from secondary particle exposure.

Criterium (3): launch and space assembly issues

The amount of mass, scale of structures, and complexity of assembly of the magnet systems must be fully understood and found

Payload System	**Characteristic**
Orion MPCV Inert Mass	14 t
Orion MPCV Propellant Capacity	8.6 t kg
Orion MPCV Specific Impulse	327.5 sec
Deep Space Habitat Mass	34 – 53 t
Space Exploration Vehicle Mass	6.5 t
SEV Stage Mass Fraction	15%
SEV Propulsion Stage Isp	355 sec
Mars Lander – short-stay missions	113 t
Mars Lander – long-stay missions	89 t (ea)
Propulsion System	**Characteristic**
Cryogenic Propulsion Stage	
Mass Fraction	23%
Specific Impulse	465 sec
Nuclear Thermal Propulsion	
Core Stage Mass	21 t
Drop Tank Fraction	26%
Specific Impulse	900 sec
Electric Propulsion	
SEP Specific Mass	30 kg/kW
NEP Specific Mass	20 kg/kW
Specific Impulse	1800 - 6000 sec
Propellant Tank Fraction	5%

Figure 17. Payload and Propulsion System Design Characteristic Assumptions. Data from Mars Design Reference Architecture (DRA) 5.0 – Addendum #2

reasonable as the cost of access to space is still the determining factor in any assessment of magnetic shielding feasibility. All three of the concepts described in section III will require some form of space assembly. While this is not a show stopper in and of itself, it does make it more difficult to justify the cost without some additional benefit. There is no real benefit other than reduction in GCR exposure for the ESA toroid and the NASA 6-1 solenoids. Given that the systems are larger and likely more massive than the habitat they are protecting, along with lack of significant protection, it is highly unlikely that these systems would ever be adopted. Mass estimations and possible implementation strategies were made for both approaches. From these analyses, that with the reduction in field required for the DTM, along with the supporting framework for the HTSC coils can be integrated into the spacecraft external wall structure, it should be possible to deploy the DTM without a significant mass penalty. This needs however to be more critically evaluated.

The DTM habitat volume was made similar to that proposed in the DRA-5 manned Mars mission studies (~ 500 m^3). In order to evaluate the shielding mass as a fraction of the total mass required in LEO, it is worth examining the expected masses for the major components taken from the most recent DRA-5 2nd addendum [12] and shown in Fig. 17.

It is clear that the habitat component is far from being the driving factor in the total mass. The total mass for the Mars mission is dependent on many factors, the primary ones being mission duration, length of stay, and type of propulsion employed. These are nicely summed up in Fig. 18, also taken from the DRA-5 Addendum #2. It is evident from this analysis that long duration missions using either solar of nuclear electric propulsion can reduce the total mass in LEO to something that is less than the entire space station. It is also evident that these missions will be of long duration and will thus require the most protection from GCR. With a nominal total mass in LEO of 200 metric tons, 53 t of that is habitat (the highest end of the range shown in Fig. 17 being due to the extra space and provisions necessary for the longer duration in space.).

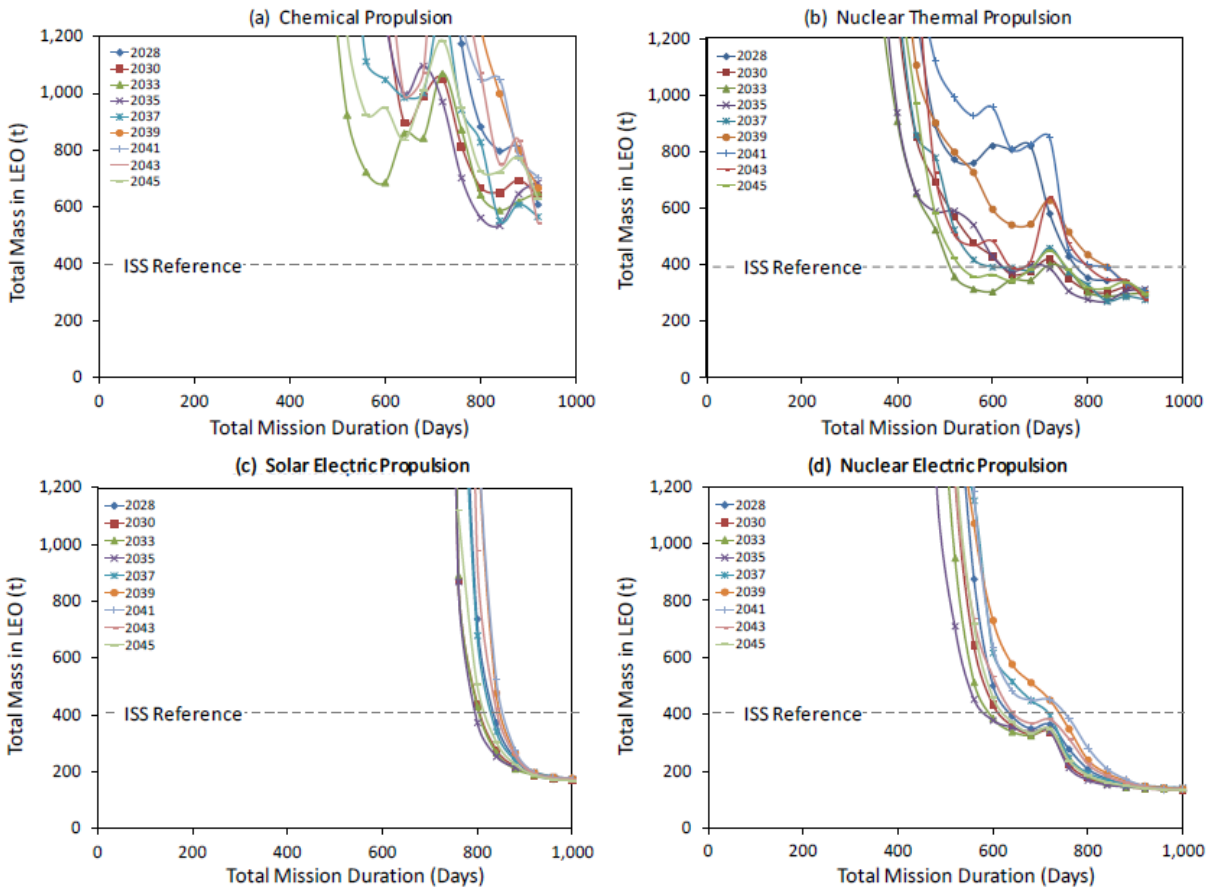

Figure 18. Sensitivity of the estimated crew vehicle mass as a function of round-trip mission duration for the short-stay, 60 days at Mars, opposition-class missions. short-stay, 60 days at Mars, opposition-class missions.

Considerable work has been done on designing the HTSC coils, cryogenic systems and structural elements that would be needed for both the ESA toroid and the NASA 6-1 solenoids. The latter had the additional issues of extensible magnets that required both inflation and massive stabilizers for all 6 of the large solenoids as well as radiators due to the large footprint of the entire HTSC system.

The need for flexible HTSC coils made yttrium-barium-copper-oxide (YBCO) the only suitable choice. The major alternative, magnesium diboride (MgB_2), has a much lower mass density (2.6 g/cm^3 vs 6.3 g/cm^3), but has limited flexibility, which is not an issue for either the ESA Toroid or the DTM. The MgB_2 HTSC was the choice for the ESA toroid as there was great experience and considerable development of HTSC wires and cables with this material from studies conducted for the HTSC magnets used at CERN on the Hadron Collider [13]. As flexibility is not a major concern, the DTM HTSC coils would likely be made from MgB_2 cables similar to those shown in Fig. 19 taken from Ref 13. These cables have been made in 20 m lengths capable of carrying 20 kA/mm^2.

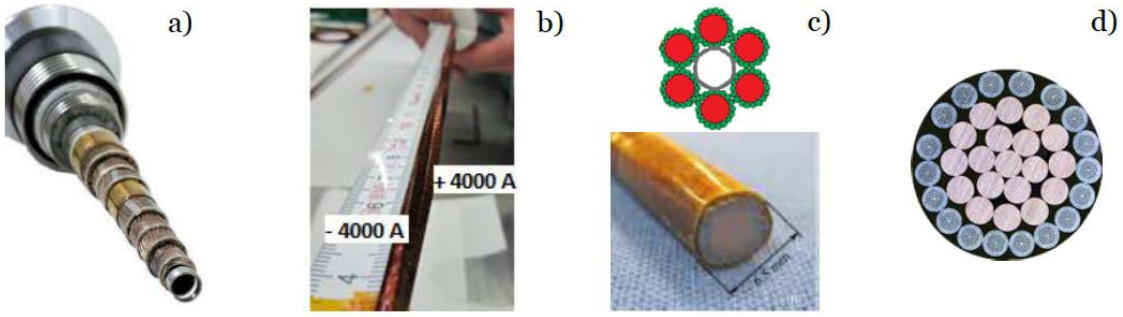

Figure 19. MgB_2 cables. From left: a) prototype power transmission cable made from MgB2 tape (~ 3,000 A DC at 20 K, Diam ~ 30 mm); b) twisted-pair cable made from MgB2 tape (~ 4,000 A DC at 4.2 K, Diam ~ 5 mm); c) top: prototype cable (consisting of six sub-cables) made from round MgB2 wire (20,000 A DC at 24 K, Diam ~ 20 mm); bottom: one of the six sub-cables each made from 18 MgB2 wires, of 1 mm diameter, helically wound around a copper core; All quoted critical currents are in self-field conditions (~ 1 T).

One can now calculate the mass of the HTSC coils for the DTM given the mean toroidal circumference ($2 \cdot \pi \cdot R$ = 75.4 m or 7,540 cm) and total current desired. The MgB_2 cable can carry 20 kA/mm^2 or 0.2 MA/cm^2. To achieve the shielding shown in Fig. 23 a total loop current of 12 MA was required; so that a total cross section for the cables would need to be 24 cm^2. With the density of MgB_2 stated above this yield a total HTSC mass of 470,500 grams or 0.47 t. Even taking a more conservative current density of half that assumed, the MgB_2 mass is only 1 t and is clearly not a problem by itself. In fact, a factor of 10 reduction in current density (2 kA/mm^2) would still not make the HTSC mass a significant problem. There is however the mass of the cable reinforcement and structures required to support the magnetic hoop forces. As a guide to estimating these additional masses, it is useful to see what was done for the two other concepts in this regard. The NASA 6-1 solenoids are enormous, use a more massive HTSC, requires self-inflation, and has difficult cooling requirements. None of which apply to either the ESA toroid or the DTM. It was also estimated that the mass of the NASA 6-1 solenoid system was close to three times that required for the ESA Toroid [1]. As the ESA Toroid concept is similar to that of the DTM at least in scale and material, it is worth examining what their mass analysis concluded [14].

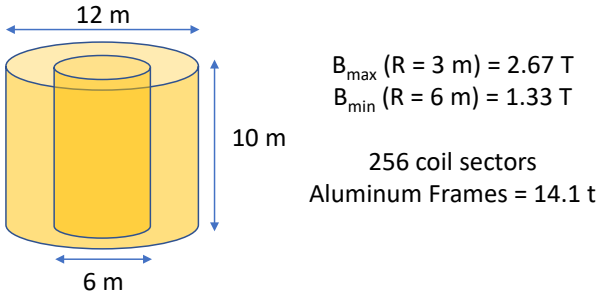

Figure 20. Evaluation of the structural mass needed for the ESA magnetic shield based on a large, continuous toroid with a wide habitat comprised of with 256 sectors. From Ref. 14.

In the ESA analysis a larger toroidal magnet system was considered with the

dimensions shown in Fig. 20. It was estimated that the mass of the Aluminum frames required to support the magnetic forces was roughly 14 t. The assumed magnetic fields indicated in Fig. 20 are larger by roughly a factor of two than that required for the DTM (see Fig. 10). Additionally, the volume of the magnet is 850 m^3 which is significantly larger than the DTM (520 m^2) which is roughly the size of the habitat. The magnetic forces on the support structures scale as B^2, and this alone would reduce the required mass by at least a factor of four not counting any reduction from the spacecraft structure or the smaller magnet volume. It would appear that additional spacecraft structural reinforcement on the order of 4 t would provide more than adequate support for the DTM coils. This plus the HTSC coils would add up to 5 t. There will also be cooling systems, power-up supplies, possible additional support systems, as well as contingency mass as this estimation is hardly a design review. A conservative doubling of the 5 t to 10 t should cover these additional concerns. Even with this extra mass, the total is far from prohibitive based on the numbers for the total mass in LEO shown in Fig. 18 for the DRA5 manned Mars mission designs.

Criterium (4) Advantages beyond GCR protection.

Given the likelihood of a significant additional expense to incorporate an active magnetic shielding system, it would go a long way toward adoption if there were other benefits from other uses for the shield beside crew protection that would help justify the investment in the shield deployment.

The major health hazards of spaceflight, in addition to the high levels of damaging radiation, include the absence of gravity, long periods of isolation and confinement, a closed and potentially hostile living environment, and the stress associated with being a long distance from Earth [10].

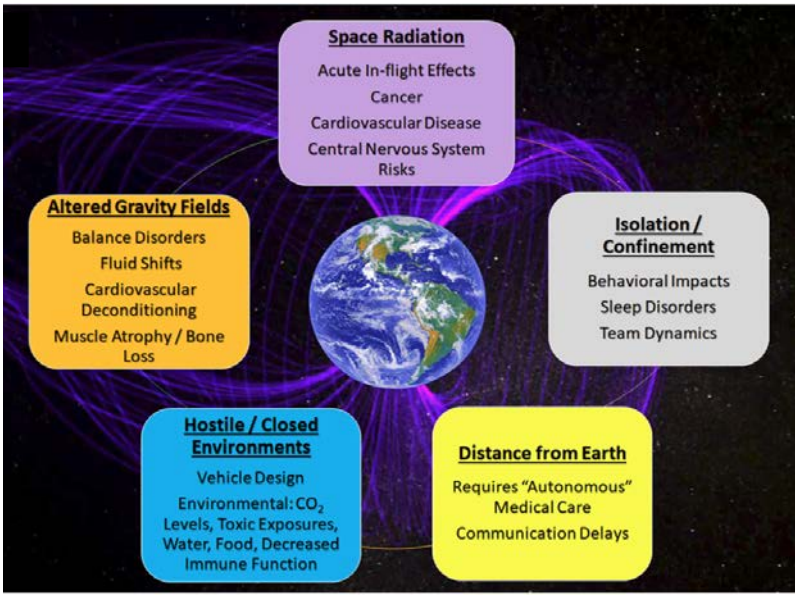

Figure 21. The five main hazards of spaceflight. The key threats to human health and performance associated with spaceflight are radiation, altered gravity fields, hostile and closed environments, distance from Earth, and isolation and confinement (figure from Ref. 10),

Each of these threats is associated with its own set of physiological and performance risks to the crew that must be adequately characterized and sufficiently mitigated (see Fig. 21). Three of the hazards relate to the health measures that can be addressed by extensions of the efforts that are currently being practiced on the International Space Station. The solutions to these are more in the realm of space medicine as they deal primarily on human physiology. Long term exposure to both space radiation and the microgravity environment of deep space however are more amenable to elimination by spacecraft design modifications such as the GCR shielding described here. It is clear that a toroidal design for the spacecraft at a sufficiently large radius such as the DTM provides for a means to create artificial gravity by simply rotating the spacecraft in the toroidal direction. In this manner both the issues of space radiation and the negative effects of microgravity can be ameliorated. The small cylindrical habitat radii of the 6-1 Solenoids and the ESA Toroid are not amenable to such a centripetal gravitational force as the artificial gravity. For one, there would be a strong gravitational gradient across the habitat. One could have their head at no gravity and their feet

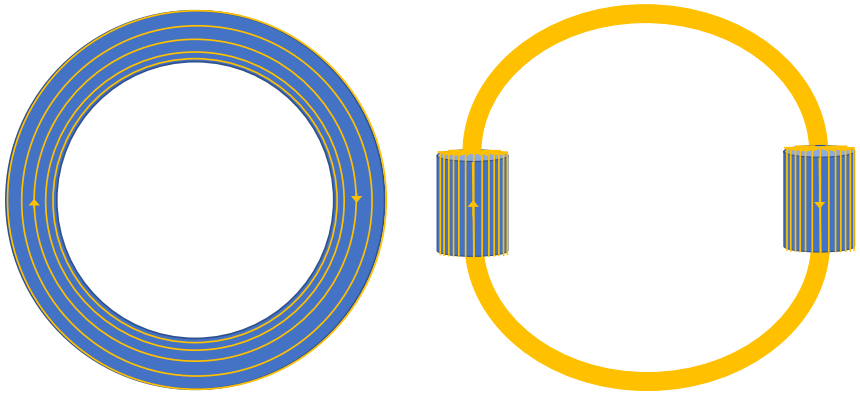

Figure 22. Example of an alternate DTM Geometry (right) for accommodating a traditional habitat design such as DRA5. Dipolar Toroidal Magnetospheres can be formed with a wide range of crew habitat geometries.

firmly planted with unknown physiological consequences, not to mention the strong Coriolis force that would make carrying out any motional task extremely difficult. Anyone who has ridden the “Gravitron” at a carnival can attest to this difficulty.

It would appear that virtually all spacecraft designs start with a cylindrical shell. This bias is not warranted given the fact that any deep space voyage will require extensive space assembly at least as significant as that of the ISS. A picture of the ISS should convince anyone that the habitat shape does not need to be a can. The DTM can be made more amenable to can shaped habitats if that is thought to be necessary. An illustration of which can be found in Fig. 22. The geometry that was employed in the tests and the initial particle tracing analysis was the simple circular torus seen on the left in Fig. 22. A straight forward way of including any habitat design that has been previously considered at NASA and elsewhere is to make two modules with possibly shorter length

or smaller diameter to keep the toroid balanced and the total volume and costs similar. These modules would be positioned at 180° from each other connected by a conduit that continues the HTSC toroidal currents. Having more modules is certainly feasible. With two, the artificial gravity can be provided by rotation of the two modules about an axis in the up/down direction in Fig. 22, which is different than that in the toroidal direction as would done for the azimuthally uniform torus. The hoop force from the magnetic dipole field is stabilizing so that an inflatable conduit can be considered. A rigid connecting tube can be made with sufficient diameter to accommodate travel between the two modules. As the magnetic field exterior to these tubes will be larger, the shielding should be better here. These tubes are field free and could be used as sleeping quarters, mess etc. so that a lower field energy and thus conductor mass could be employed. The shielding for a geometry such as the one on the right in Fig. 22 was tested with the Lorentz 3D particle trajectory code and proved to be somewhat better than a continuous toroid of larger diameter, primarily due to the higher surface fields in the connectors and smaller cross section for GCR exposure.

It should be mentioned that there is another major benefit to a large-scale open magnetic dipole structure such as the DTM. It has to do with the concept of aerobraking and aerocapture for decelerating the spacecraft in the upper regions of planetary atmospheres as it approaches a planetary body, and thereby capture it in a stable orbit

The novel device that has been investigated to accomplish this kind of aerobraking is referred to as a Plasma Magnetospheric Shell (PMS). It is based on the drag encountered with the neutral particles in the planetary atmosphere by a spacecraft-sourced plasma confined inside a dipolar magnetosphere. The magnetic field requirement for the dipole coils anchored to the spacecraft for the PMS concept to work is considerably less than that generated by the DTM for shielding, so that in addition to performing just aerobraking, aerocapture is well within the range of the higher drag required. This demanding task using the high-field PMS dipole is referred to as Magneto-AeroCapture (MAC), and is similar to that performed now by a solid deflector or aeroshell to perform high dynamic pressure atmospheric braking. An outline of the process can be found in Fig. 23. The use of such a braking mechanism dramatically reduces the propulsion and fuel requirements for planetary orbital maneuvers. There are several unique advantages to PMS braking: 1) Magnetoshell drag >> Aerodynamic drag. Even though the PMS is deployed at higher altitude with lower neutral density the scale of the PMS is considerably larger. 2) Neutral-plasma drag >> Plasma-plasma drag. Even though the magnetic field can directly deflect charged particles, the number density of neutrals in most planetary atmospheres, including the Earth, is several orders of magnitude greater than the plasma density. 3) Drag can be controlled electronically in real time. The time to change the plasma fill density is less than a second, so that the interaction with the neutral flow can be modulated as the atmospheric neutral density (hence drag force) changes. 4) Same Delta-V savings as inflatables, but without heating concerns. The kinetic energy of the directed atmospheric particle flow is dissipated in the form of a higher plasma dipole ion and electron plasma temperature (neutral flow stagnation temperatures will be 5 – 20 eV for most

planetary spacecraft insertion velocities). 5) The plasma mass required is less than a few grams. The magnetic coils needed for the PMS are already onboard for GCR shielding. The PMS concept

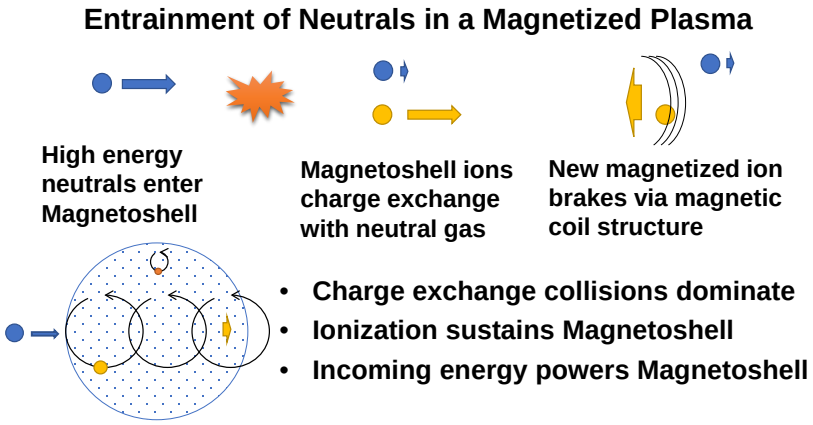

Figure 23. Key Physics behind the Plasma MagnetoShell (PMS) concept. The process is as follows: 1) A spacecraft has or deploys Magnetoshell hardware on a tether. 2) A sub-Tesla magnetic dipole field is generated. 3) An RF generated, low-temperature, magnetized plasma is created in that field. 4) Plasma interacts with atmospheric neutrals through charge-exchange and collisions, 5) The captured particles transfer directed momentum to dipole through field line bending and equilibrate; thereby decelerate the spacecraft. 6) Dipolar plasma is both refueled and maintained by captured planetary neutrals.

and related technology that was developed at MSNW with funding from the NASA Institute for Advanced Concepts (NIAC). The results of the study indicated that a low-cost, low-risk aerocapture was feasible for a range of Earth and deep space missions [15].

By using aerodynamic forces, a spacecraft can perform orbit insertion, orbit lowering, or re-entry with little to no propellant. PMS takes aerocapture one step further by eliminating the massive aeroshell. The momentum of the spacecraft is dissipated in the ambient neutral atmosphere via a low-density plasma magnetized in the dipolar field. This plasma interacts with the ambient low-density neutral population, which appears in the spacecraft frame as a directed flow, through charge exchange and collisions. After a collision, the now magnetized atmospheric ion reacts its directional momentum onto the magnet via field line bending and stretching which then decelerates the spacecraft, acting in effect like a “plasma parachute”. This plasma is formed with an electrodeless RF plasma source which injects a low temperature (~ 10 eV) magnetized plasma. With the aeroshell now being composed of a massless magnetic field, the scale of the shell can be as large as 100 meters while requiring only a gram of plasma. Frictional heating would no longer be of concern as the energy dissipation required to slow the spacecraft would be deposited into the plasma ions helping to maintain the MagnetoShell Plasma. In the NIAC study, a 1.6 meter PMS generated by a 10 cm diameter coil dipole coil set demonstrated an increased drag force from a supersonic flowing Argon neutral jet by 1000X (see Fig. 24).

As mentioned, the dipolar magnetic field generating capabilities of the DTM shield would be more than sufficient for any aerocapture scenario. It would allow for orbit insertion at very high

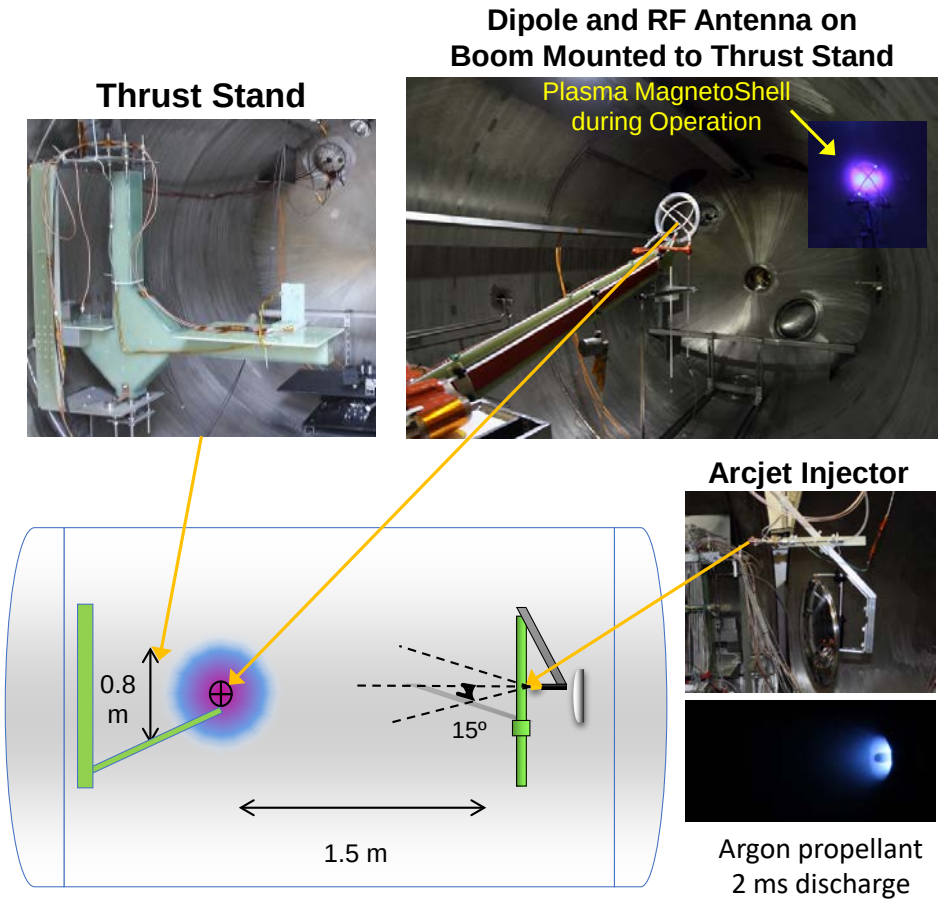

Figure 24. Experimental Demonstration of the PMS at laboratory scale. Methodology: Employ MSNW 4m x 2m vacuum chamber 23,000 l/s pumping to maintain spacelike conditions. Install Argon arcjet (few % ionization) at one end to deliver a high velocity (~ 2 km/s) neutral gas surrogate. Construct a small scale ~(10 cm) dipolar magnet w transverse RF coils to generate a Magneto-Shell Plasma confined in the dipole field. Mount the coil set with a gas and electrical feed on a boom attached to a thrust stand. Measure the increase in drag force induced on the PMS from the flowing Ar stream with and without PMS plasma.

ΔV thus allowing for much shorter trip times and payload mass fraction than conventional aerocapture techniques or aeroshells alone.

6. Results from the Experimental Testing and Shielding Analysis of the DTM

In order to understand the difference in shielding effectiveness between the simulations and an actual dipolar toroidal magnetosphere, it was decided to construct a subscale version of the DTM that would be characteristic of what one would actually build for space deployment, and reduce the particle energy so that the deflection could be studied at much less magnetic energy and field. The range of particle energies (several hundred eV) could be generated by conventional ion beams, and the deflection fields required for a sub-meter DTM would be in the sub-kilogauss range. For the ion beam to propagate the several meters required, the testing would have to be done in vacuo so that a large vacuum chamber was required, and fortunately, MSNW had such a large vacuum chamber.

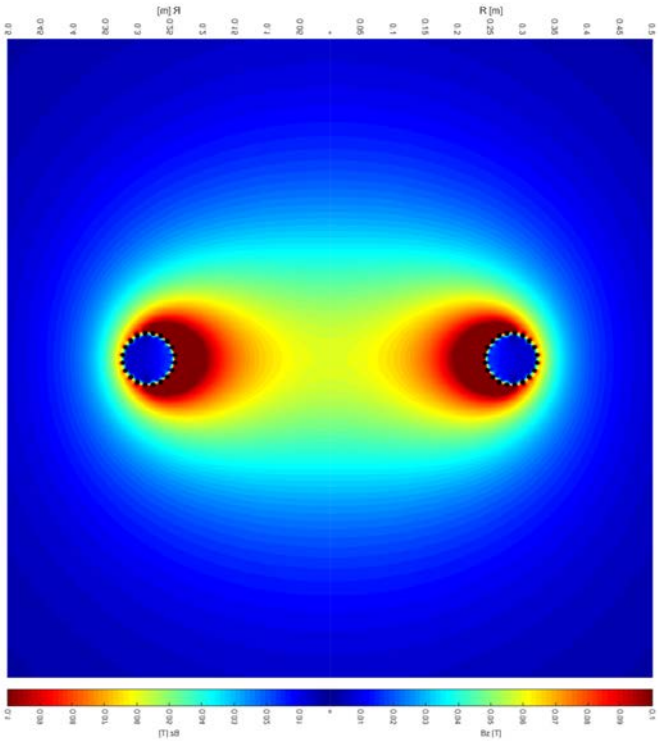

Figure 25. Magnetic field in the X-Z plane for the subscale DTM constructed for testing in the MSNW large vacuum chamber.

As discussed earlier, the toroidal current variation as a function of the poloidal angle around the minor cross section needed to be such as to cancel the magnetic field inside the torus. The magnetic field magnitude and current allocation for the anticipated experimental arrangement to be used in the testing is shown in Fig. 25. Here, an array of 20 wires were used in a parallel-series configuration that provided more current to the inner loops in order to minimize the field inside the torus when powered from a single power supply (100 V 88F supercapacitor). It was found that a much lower resistance and better insulated, braided conductor allowed for the use of only 10 flat straps. The flat straps were also closer to the geometry of the HTSC that would be used on the spacecraft. Given azimuthal symmetry of the DTM it is only necessary to obtain the behavior of the protons at a single given location on the toroid. At this location the GCR appear as coming uniformly from all altitude and azimuthal angles.

A sample of particle trajectories for the experimental geometry and fields can be found in Fig. 26. the protons are all located in the in the X-Z plane. While a plot can be made for planes at various azimuthal angles in one calculation, the “blizzard” of traces (e.g., see Fig. 7) makes it very

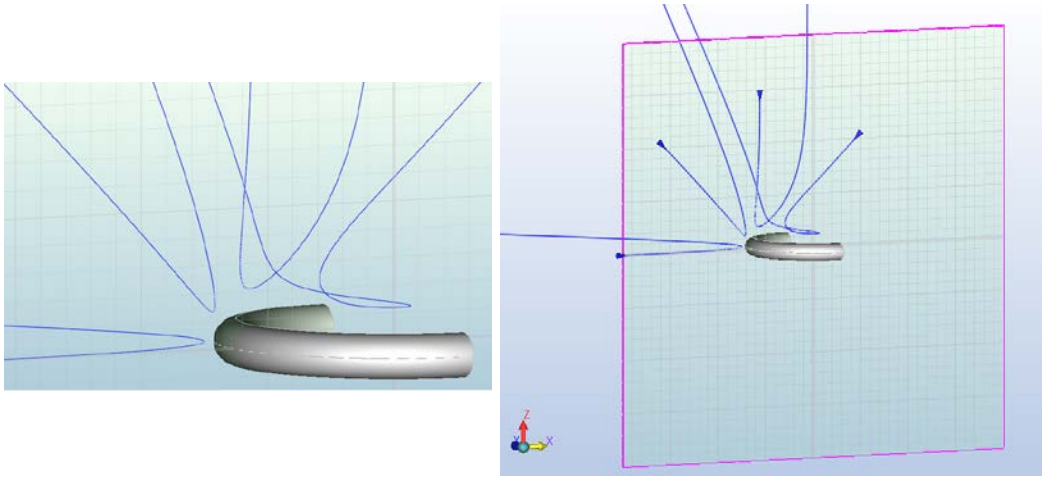

Figure 26. (right) Trajectories of four protons directed towards a specific point on the torus midplane. (left) Close-up near DTM. All protons have the same directional energy (600 eV).

difficult to understand the proton motion and trajectories. By selecting a series of starting points and planes one is able to obtain detailed information on the behavior of the GCR near the torus. In this way it can be easily determined which directions the DTM offers the best protection, as well as the direction of GCR particles to which the DTM is most vulnerable. Given the latter information, it may be possible to provide additional directional shielding in sensitive locations inside the DTM such as the crew sleeping quarters. As can be seen in Fig. 26, no particle reaches the surface of the torus with the trajectory of the proton entering radially in the midplane getting the closest to the DTM.

The testing of the DTM at MSNW in the large vacuum chamber was undertaken and was

Figure 27. Magnetic field B_{00} calibration setup. High current cable leads can be seen on the vacuum tank floor. An array of 12 Faraday cups were positioned around the torus to collect the 600 eV protons from the ion beam.

successfully completed. A brief review of the experimental arrangement for most of the data taking will be given. It was found from the particle trajectory analysis with the Lorentz 3D code, that the particles with the greatest penetration depth into the DTM came from trajectories that were initiated in the plane of symmetry (Z = 0 in cylindrical coordinates). As it did not matter as to azimuthal angle due to magnetic field and DTM symmetry, the ion beam was moved to be in this plane and aimed directly at the subscale DTM as shown in Fig. 27. The beam source in this configuration could be backed off along the axis of the vacuum tank and thus afforded the farthest placement of the source from the DTM which was positioned near the entrance to the chamber. This provided for the increased effect from the external fields of the DTM which, as mentioned earlier, was found to be significant for launch points that are only a few DTM diameters away.

A supercapacitor power supply has a very low impedance which allowed for the flow of the large currents needed. To turn on and off such a high current in such a large inductive load, a high power, high voltage (1700 V) IGBT with a peak current capability of 18 kA was employed as the

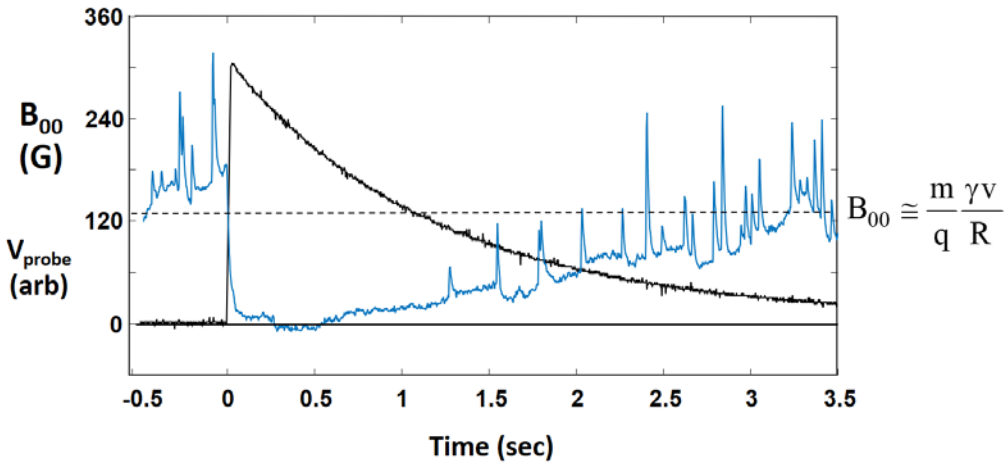

Figure 28. Results for In-Plane 600 eV Ion Beam at 75 cm (position as in picture in Fig. 26). Results indicate better than expected shielding than that inferred from analytic scaling.

switch. The safest operation was to allow for the supercapacitor to completely discharge on each pulse. It turned out that this was actually an optimal mode of operation as will be discussed. The behavior of the DTM coil, which is shown in Fig. 27, was quite reproducible. After the DTM was installed and connected up for operation, the last task was to install a hall probe at the center of the DTM to directly measure B_{00}. As can be seen in Fig. 27.

With the long decay of the magnetic field (see Fig. 28), it was possible to observe the beam current reaching the Faraday cup detector array inside the DTM as the magnetic field decayed to lower magnitude. Thus, in just one pulse the entire range of the shielding effect of the DTM magnetic field could be obtained. Typical results are shown in Fig. 28. A voltage probe measuring across the across the inputs to the DTM, and calibrated to the Hall B probe was used to monitor the magnetic field in time. In this plot it can be observed that detector 5 which was placed directly in line with the ion beam source received the maximum signal. The detector inside the DTM windings records a signal that when the magnetic field is zero (prior to DTM coil energization at t=0), there is both modulation of the detected beam current inside the DTM and frequent large spikes. The modulation is a consequence of the charging of the vacuum tank by the beam with a current return path through the ground system. While there was a filament emitter at the beam exit to balance and reduce the charging effect, it still persisted to some degree, As can be seen in Fig. 28, the modulation is still present to a small extent even when the beam is completely deflected

away from the DTM (0s ~ t ~1.2s) as the beam current is still being conducted to the tank wall. The spikes in the signal however were due to sputtering of the Aluminum cylindrical detectors. A tolerable level of sputtering could be obtained when the ion beam was operated at or below 600 V. The data in Fig. 28 was obtained at this voltage. There is no doubt, that it would have been possible to find a metal with a higher sputtering threshold. Tungsten or Molybdenum come to mind. It was not possible, however, to find a small cylindrical container made from these materials. Given the variability of the beam current, it was actually useful to have the spike as this was a clear indication that the beam was reaching the detectors.

As can be seen in Fig. 28, that with the rise of the magnetic field, the detected beam current immediately goes to zero. It remains more or less near zero until roughly t ~ 1.2 sec when the spikes return and there begins to be a definite rise in detected current.

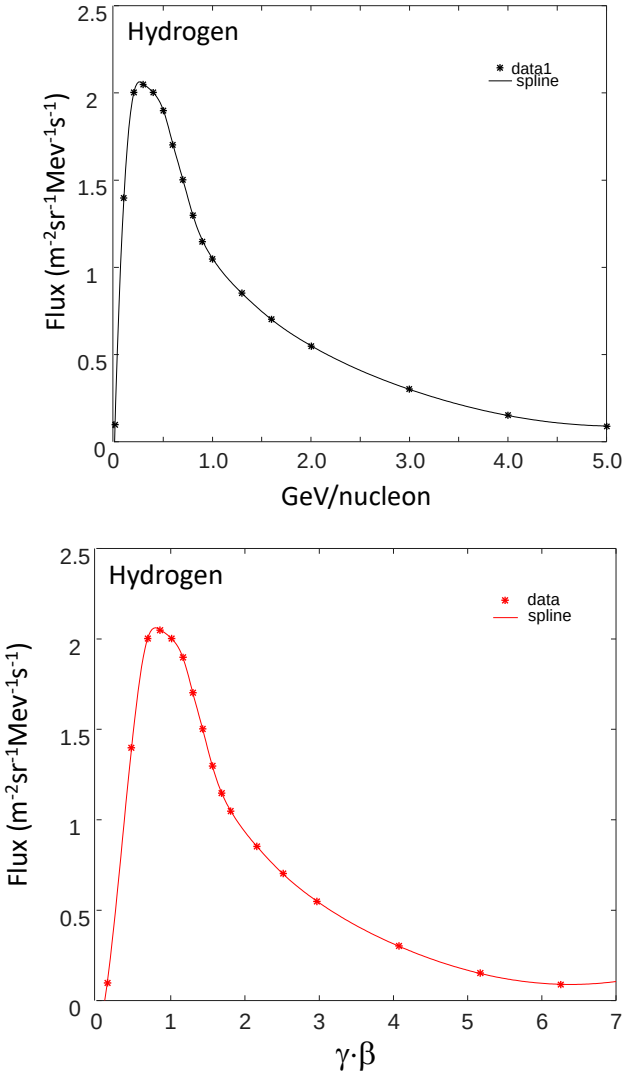

Figure 29. Linear plots for proton GCR in relevant parameters for magnetic shielding.

Clearly these subscale tests were performed at much lower energies than the GCR particles. The physics however does not change as one scales to larger size and energy. The protection observed needs to be stated in terms of a set of independent variables that characterize the deflection as a function of particle energy, charge to mass ratio of the GCR, and the radius and characteristic magnetic field strength of the DTM in the plane of the DTM at the axis of symmetry (B_{00}). The GCR have typically relativistic energies, so this must be taken into account as well. Recall that the condition for complete deflection of the GCR for the DTM one has:

$$B_{00} = C_B \frac{m_0}{qR} \gamma\beta c, \qquad (9)$$

where C_B is a constant depending on toroid geometry, R is the major radius of the toroid, m_0 is the GCR particle rest mass, and q its charge. $\beta = v_\perp/c$. It is useful to write the relation for γ and β as:

$$\gamma = \frac{E_{tot}}{m_0 c^2} = \frac{E_k + E_0}{m_0 c^2} = \frac{E_k}{m_0 c^2} + 1, \tag{10}$$

$$\beta = \sqrt{1 - \frac{1}{\gamma^2}} \tag{11}$$

where E_{tot} is the total particle energy, and E_k is the kinetic component that is commonly used to characterize the GCR particle, and typically in units of GeV (1 GeV = 1.602×10^{-10} Joules).

For a toroid with an aspect ratio of 7 and a radius of 0.28 m, as it was in the subscale tests, and given the magnetic field where shielding starts to become less than complete. From Fig. 28, one finds that $C_B \sim 1$. As seen before in the particle trajectory work, the attenuating effect of the dipole fields extend to larger energies (or equivalently to smaller field in Fig. 28), not vanishing until the particle energy is over a factor of two larger than the threshold value indicated in Fig. 28 and Eq. (9).

In order to evaluate the effect of the DTM on GCR it is useful to recast the usual way the GCR flux is plotted i.e., as a log-log plot over a spectacularly large range of fluxes and particle kinetic energies (e.g., see Fig. 15). It should be noted that the particle flux drops precipitously from its peak around ~ 300 MeV. In addition to this fact, it is now being realized that the potential harm from a biological viewpoint, the most damaging GCR particles are likely to be in the range of 0.2 to 2 GeV. Replotting the Hydrogen (proton) data from Fig. 15 with an interpolant, but now on a linear scale one obtains upper graph in Fig. 29 over the GCR particle energy/nucleon of concern. As the relevant scaling parameters for the relativistic GCR are those of Eq. (9), and using Eqs. (10 and (11), the abscissa can be stated as simply $\gamma\cdot\beta$, where it is recognized that the rest energy of a nucleon (proton or neutron) is, $E_k^{nuc} = m_0c^2 \approx 0.94$ GeV. The same data for Hydrogen shown in the upper plot of Fig. 29, but as a function of $\gamma\cdot\beta$ is found below the Hydrogen plot. From Eqs. (10) and (11) one can see that for large gamma the relationship between E_k and $\gamma\cdot\beta$ is linear. However, in the range

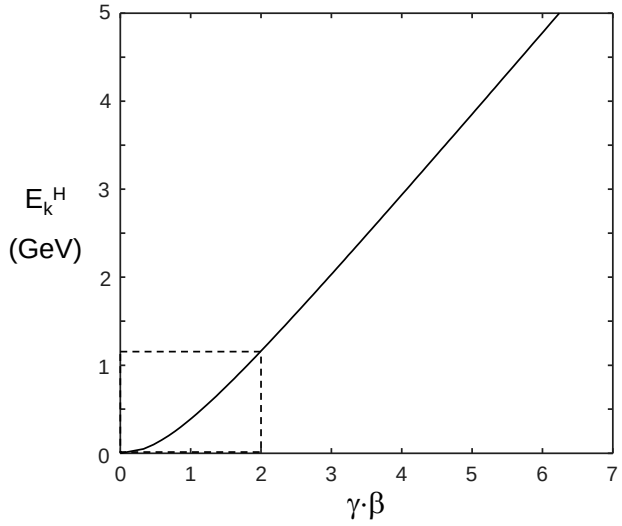

Figure 30. Relativistic proton energy as a function γ·β.

of the highest flux of GCR (0.05 to 2 GeV) it is not. As an aid for conversion form the usual MeV/nucleon abscissa, a plot of E_k as a function of $\gamma\cdot\beta$ is found in Fig. 30.

It is now possible to calculate the effect on the GCR spectrum for a 10 m radius torus with an aspect ratio of 7 carrying sufficient current to provide a B_{00} = 0.64 T, which for Hydrogen using Eq. (9) with $C_B \sim 1$, corresponds to a value of $\gamma\cdot\beta = 2$ for the full deflection of Hydrogen GCR with values of $\gamma\cdot\beta$ equal to and less than 2 (or equivalently $\leq$ 1.2 GeV). The attenuation of the GCR then tapers off over the first octave of higher energies to eventually no attenuation.

The plots for the principal bad actors: Hydrogen, Carbon, and Iron are shown in Fig.31. One can see that for a fairly modest magnetic field, the shielding of GCR can be quite effective with the DTM. If one increases B_{00} = 1 T the results are even more notable as this extends the attenuation to the point where the natural falloff in flux reaches a low enough level that the remaining GCR that get through is negligible.

It should be noted that the protection indicated by the experimental results is roughly a factor of two better than the calculations discussed earlier. At first it was thought that the improvement could be due to the small changes in aspect ratio of the habitat shape in going from circular to elliptical. Further calculations showed that these changes made only small differences. It should be recalled that all of the concept comparison was performed with uniform and continuous sheet currents. This was done primarily due to the fact that both the

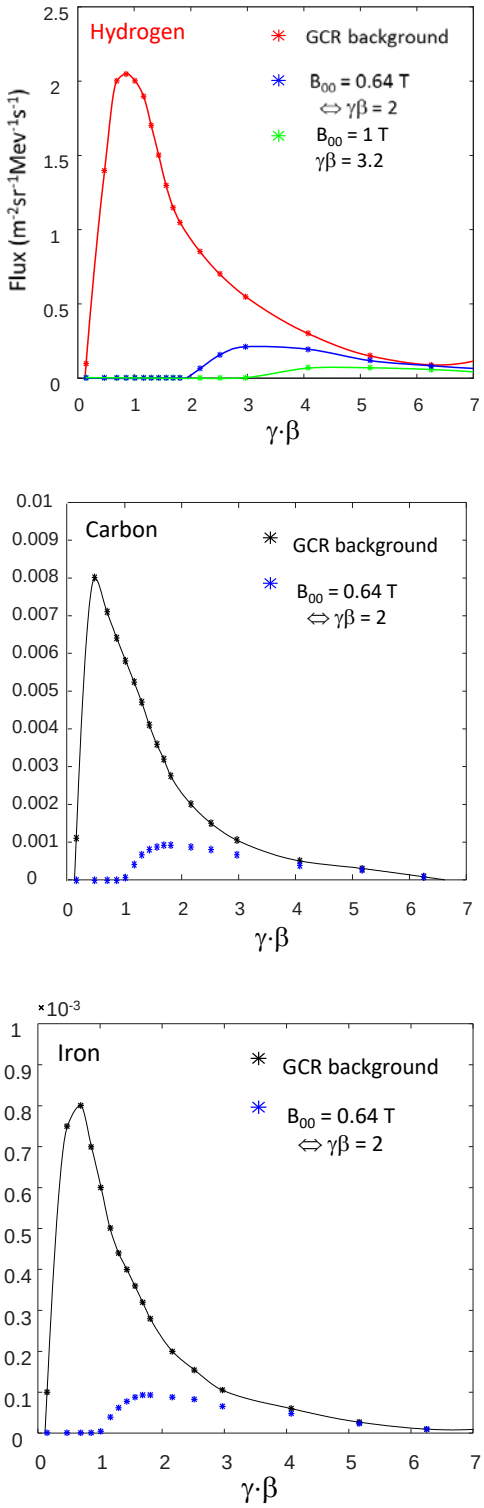

Figure 31. Predicted attenuation of the GCR spectrum from a Dipolar Toroidal Magnetosphere (DTM) where the toroid radius is 10 m and the aspect ratio = 7.0.

ESA toroid and the 6-1 solenoids had assumed this current distribution in their shielding analyses. For the experiment, however, the current was concentrated in distinct bands of current carriers (10 in all) separated by gaps of slightly larger extent. It was thought that this would aid in protecting the coils themselves as well as provide port access in the habitat for space observation, solar power input, communications, etc. It turns out that this was a fortuitous choice as will now be discussed

Numerical Calculation of GCR Behavior Near a Coil

The desire here was to evaluate the local behavior of the GCR near the HTSC coils. The 3D Monte Carlo codes employed in previous efforts elsewhere [7] were not an option as they would not be adequate to resolve the particle motion to the accuracy desired in the near field of the coils as the GCR approach the current conductors. There is one very important advantage that came from the original numerical work performed with the MSNW code in that the resolution could be enhanced in such a way so that details of the particle's trajectory within the magnets could be analyzed. It was clear from the analyses by other groups employing the Geant 3 and 4 codes [1,8] that the interception of the GCR by various structures can be quite deleterious (see Fig. 5). It is worth recalling that with the DTM, the large deflecting magnetic fields reside *outside* the conductors and should therefore offer significant protection for the coils themselves. As this effect

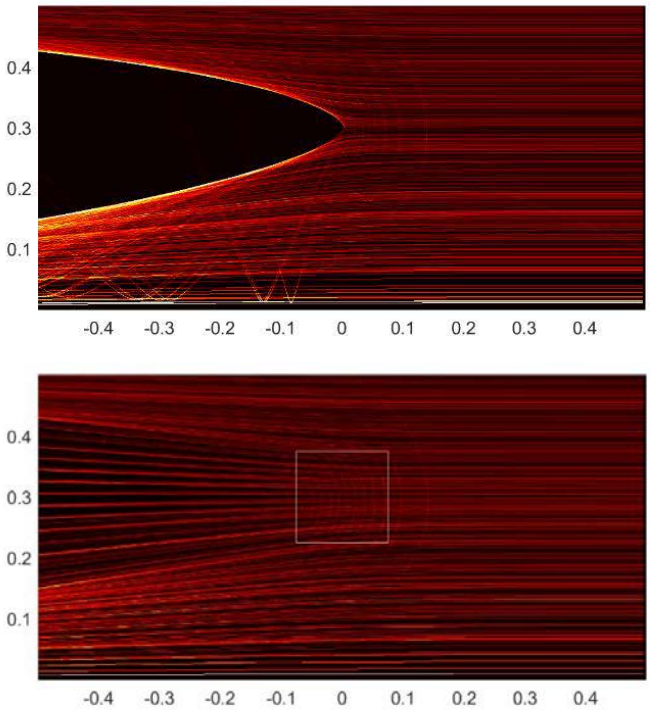

Figure 32. The figures above showing the difference in particle trajectory for a single large current bundle (top) as compared with a 15 × 15 grid with the same total current (bottom). Proper coil concentration and current distribution can help protect from and redirect GCR away from coils.

concerns the very local behavior of the GCR particle in the near field of the coils, the code was modified to analyze this effect.

Given the fact that the field near the coil is at its peak magnitude just outside the coil, one would expect that there would be a significant local deflection of the GCR possibly keeping the GCR from striking the coils. This in fact was borne out by the high-resolution trajectory calculations where the initial GeV nucleons were directed at the coils, and where the strength of the magnetic field was insufficient to deflect the particles completely away from the habitat (see Fig.32). While there is little concern with damage to the coils from the GCR as the energy flux is miniscule, it would be advantageous to keep the magnet currents in bundles or cables as this will minimize daughter particles from being generated from collisions of the highest energy GCR with the coils.

As Fig. 32 clearly shows, the protection of the coils is enhanced by local current concentrations rather than a uniform distribution. What wasn't immediately obvious was whether this bundling and would provide for a more effective shield for the same total current. The Lorentz 3D code calculations for the DTM described earlier were repeated but this time with twenty cablelike bands as current carriers. This was done with an overall transparency of 50% similar to the experiments. The cross-sectional volumes were proportional to the current required at that poloidal position to null the field inside the habitat. The total sum of all 20 currents was kept the same as the total surface current used in Section III for the comparison. The result was roughly a factor of two improvement in the shielding effectiveness, which was now in line with what was observed in the experiments.

7. Application of the ESA Toroid Concept to the NASA DRA5 Module Design

It is clear that adopting the DTM that has been analyzed up to this point as a Deep Space Habitat (DSH) would require a significantly different space habitat than anything that NASA has considered in the past. Given that the DTM is a feasible, cost-effective, and more advantageous approach to GCR protection for humans, in addition to the fact there is no other reasonable paths at this point, one must consider whether it is worth a change in scope to include a DTM to protect humans from GCR. Something that could possibly be more important for the health and well-being of the astronauts is the fact that the DTM would provide for a simple way to create an artificial gravity. Given that the much less-challenging plans that have been developed such as those associated with DRA5, despite the fact they will most likely not be viable from a human health and safety point of view, it is worth examining what one might be able to do with magnetic field protection given the constraints of the typical designs that have been already generated. Such an effort was undertaken using the SLS Derived Module which was part of the Deep Space Gateway design study. A summary of this module is shown in Fig. 33.

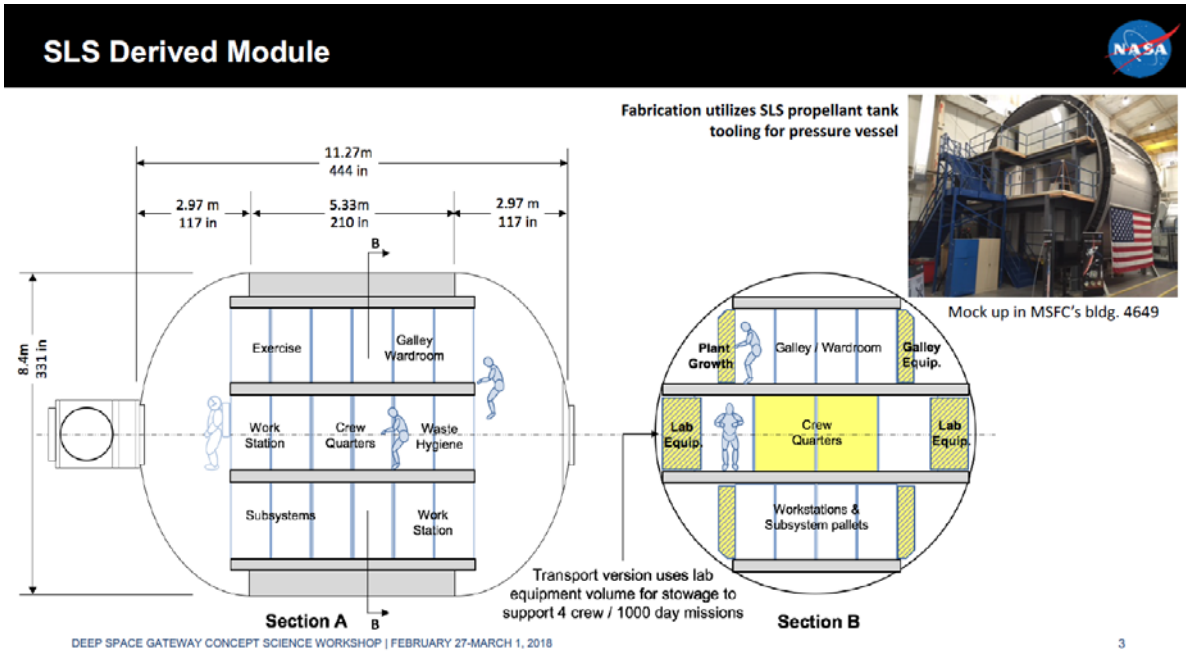

Figure 33. Proposed habitat and scientific laboratory for deep space missions.

It is worth noting that the performance of the magnetic field shielding found in the comparison study of section III, there is the possibility of employing a toroidal coil set for the generation of a closed field topology (it is noted that all magnetic field lines are closed, but in this case within the coil boundary). The Achilles heel of employing a simple circular or elongated cross section toroid is the lack of protection to GCR particles either directed or deflected into the polar regions of the habitat where there is little if any magnetic field perpendicular to the trajectory of the particles, thus allowing easy passage into the habitat. The idea here is to shape the toroid to minimize this

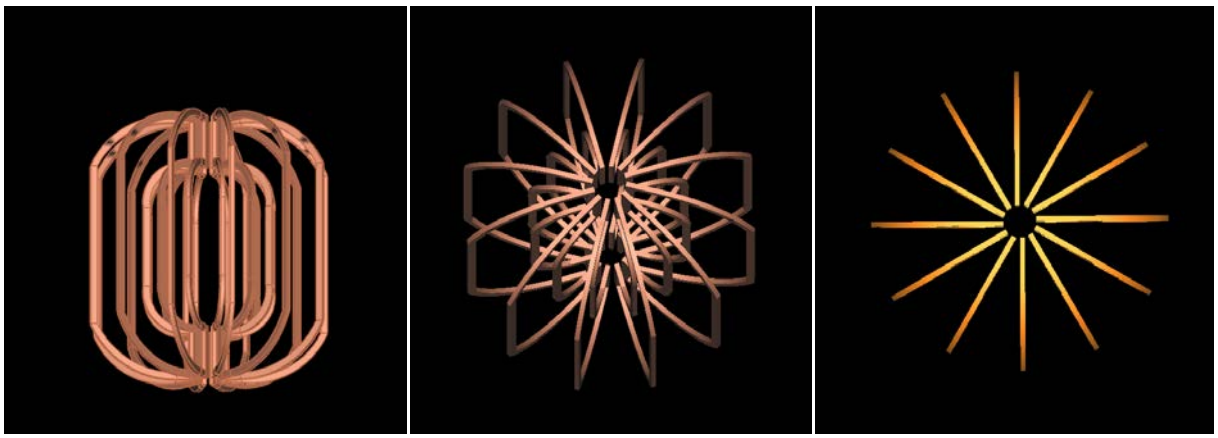

Figure 34. Three views of the prototype coil set for creating a toroidal magnetic field surrounding the habitat module of Fig. 33.

opening as well as position a small torus of the DTM variety at each of the two axial openings (see Fig.34). The coil design was constrained at this point to a size that could fit into the faring of the rocket similar to the one used to launch the SLS Derived Module shown in Fig. 33. This would allow for the magnet and supporting casing structure to be fabricated on Earth for easy assembly in space, thereby avoiding issues involved with magnet inflation and deployment that had plagued previous magnetic shielding concepts. The first step was to consider the toroid that would most likely give the best shielding from all directions.

A module of a prototype coil set for application to the SRS Derived Module has been made. By having the toroid shape be concave allowing the coils to wrap around the ends of the module provides for substantial shielding of GCR coming in from the ends of the module. A fully populated toroid with twelve coils as shown in Fig. 34. As can be seen in Fig. 34 that the shape of the conductors for the toroidal field reach down close to the axis at each end providing end protection. It is believed that the set of essentially 12 dipole field coils combined into an array will allow for a significant external field concentrated around each coil.

While it would be possible to arrange for another coil set, for example a pair of saddle coils that would effectively deflect particles from entering along the axis, it was decided that initially only the toroidal field coils would be energized and their effects on the entire 4π steradians of incoming GCR would be characterized. A magnetic field vector plot in the midplane of the toroidal coils is shown in Fig. 35. It can be seen that the field vanishes as desired inside the region to be occupied by the habitat. The open nature of the toroid allows for the magnetic field to extend considerably

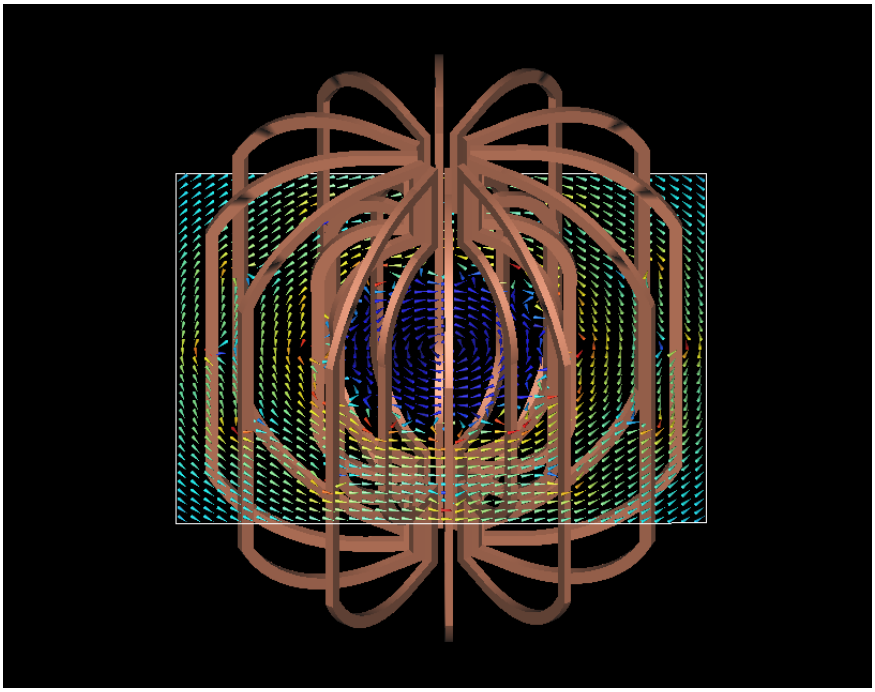

Figure 35. Magnetic field vector plot in the midplane of the shielding toroid coil set.

outside the toroid as well as concentrates the currents into discrete segments so that the positive effects described in the discussion of Fig.32 should be generated here. The very open arrangement also minimizes coil interactions with the GCR. While the inner coils are much closer together, there should have been a significant reduction or redirection by the toroidal fields by that point. It is also important for keeping the local magnetic fields surrounding the coils from penetrating too far into the space habitat.

The difference in the magnetic fields from the original ESA toroids that employed a near continuous array of poloidal currents thereby keeping the toroidal magnetic field inside the torus,

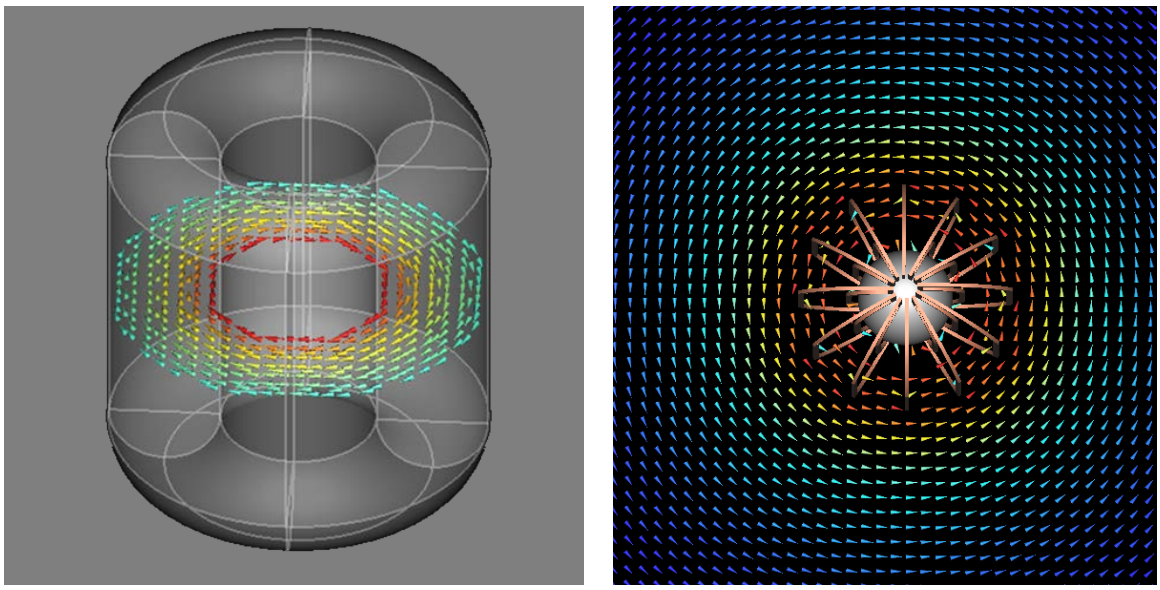

Figure 36. (Left) Magnetic field vector plot in midplane of the ESA toroid. (Right) Magnetic field vector plot in midplane of the hybrid "open" toroid. Field line are plotted for regions where the magnetic field magnitude is 5% of the peak magnetic field or larger.

to the hybrid scheme proffered here can be seen in Fig. 36. As can be seen, the magnet protecting magnetic field is now much larger outside the torus, although that is saying very little as there is essentially no external field for the ESA toroid. The magnetic field is in fact even stronger than that found for the DTM as the scale of the and volume of the toroid is much larger in this case. As was mentioned, increasing the magnet volume is always advantageous as far as efficiency of shielding (Ω) is concerned. The DRA5 scale habitat here is also much larger than that of the Columbus module assumed in the ESA shielding studies. (~ 100 vs. ~500 m^3) which further improves shielding effectiveness. This is made clear in Fig. 37. This is an expanded view of Fig. 13 with the addition of the finite current element DTM and the Hybrid DTM-Toroid shown in fig. 34. With the increased habitat size and coil volume, the shielding from the Hybrid can be shown to be quite effective in reducing the polar exposure to GCR and also very effective at shielding GCR from the "barrel" region as well. It would appear that the exposure of the coils to secondary

emission from GCR impact would also be substantially improved as the external field protection is as good if not better than the DTM. Of course, the ability to provide complete protection as in the DTM would require additional coil structures at the ends. As to the what and how will be the work of future studies. Needless to say, there would still be no way to provide an artificial gravity or planetary braking system, but this hybrid coil set would at least be consistent with the current DRA5 plans for the space habitat, and would provide for a HTSC coil profile that could fit in the fairing of a a large Aries class rocket, and then be readily assembled onto the habitat in LEO.

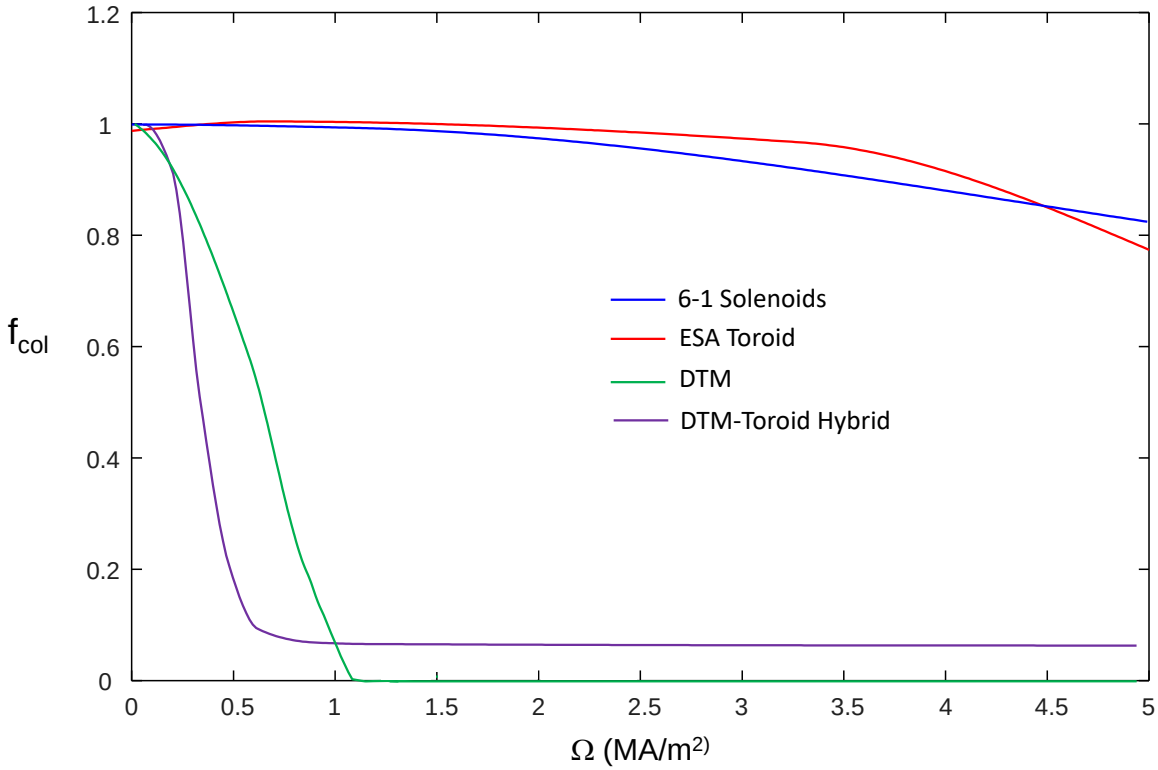

Figure 37. Fraction of 500 MeV protons reaching the habitat of the various concepts as a function of the efficiency parameter Ω..

7. Summary

An optimal magnetic shielding configuration for significantly reducing astronaut exposure to Galactic Cosmic Radiation (GCR) on long interplanetary missions has been realized, and is referred to as the Magnetospheric Dipolar Torus (DTM). This configuration was shown to have the singular ability to deflect the vast majority of the GCR including High Z Energetic (HZE) ions. This external (to the spacecraft) dipolar field is created by an array of unidirectional toroidal High Temperature Superconductor (HTSC) windings mounted externally on the surface of the toroidally-shaped spacecraft habitat so that the spacecraft directly supports the magnetic hoop forces generated by the toroidal currents. The magnitude of the toroidal currents are arranged poloidally to flow so as to maintain the spacecraft shell as a constant flux boundary where the poloidal flux $\varphi = 0$ inside the spacecraft keeping the habitat field-free. As the dipole magnetic field is perpendicular to the spacecraft habitat in all directions, the DTM provides a deflecting shield to all the incoming GCR which is nearly isotropic. In addition, the DTM shields the HTSC magnets as well thus eliminating the secondary particle irradiation hazard, which can dominate over the primary GCR for shields with closed magnetic topologies.

MSNW also developed 3-D relativistic particle code to evaluate magnetic shielding of GCR and employed a very accurate commercially available particle trajectory and magnetic field solver, Lorentz-3M, from Integrated Engineering to evaluate shielding effectiveness for the GCR spectrum encountered in space. The codes were employed to evaluate a wide range of magnetic topologies and shielding approaches including prior proposed magnetic shielding concepts. With DTM shielding it was found that both the structural and magnet mass as well as power requirements were significantly reduced. The DTM shielding effectiveness was calibrated in a large laboratory vacuum chamber experiment using a high energy beam as a surrogate for the GCR encountered in space. It was discovered that by distributing the shielding currents in discrete cables, the local field concentration provided for a better shield for the magnets themselves, as well as reduced the penetration of GCR by a factor of about one half.

References

1] Filippo Ambroglini, Roberto Battiston and William J. Burger, *Evaluation of Superconducting Magnet Shield Configurations for Long Duration Manned Space Missions*, Front. Oncol., 08 June 2016

[2] Jeffery C. Chancellor Graham B. I. Scott and Jeffrey P. Sutton, *Space Radiation: The Number One Risk to Astronaut Health, beyond Low Earth Orbit***,** Life **2014**, *4*, 491-510

[3] C. Zeitlin *et al., Measurements of Energetic Particle Radiation in Transit to Mars on the Mars Science Laboratory,* Science **340**, 1080 (2013)

[4] Shayne Westover *et al, Magnet Architectures and Active Radiation Shielding Study (MAARSS),* Final Report for NASA Innovative Advanced Concepts Phase II

[5] L.W. Townsend, *Overview of active methods for shielding spacecraft from energetic space radiation*, 1st International Workshop on Space Radiation Research and 11th Annual NASA Space Radiation Health Investigators' Workshop

[6] Lawrence W. Townsend, *Critical Analysis of Active Shielding Methods for Space Radiation Protection,* IEEAC paper #1094 (2004)

[7] Brun R, Bruyant F, Carminati F, Giani S, Maire M, McPherson A, et al. *Geant – Detector Description and Simulator Tool*. Geneva: CERN Program Library Long Write-up W5013, CERN (1994). p. 430.

[8] Agostinelli S, Allison J, Amako K, Apostolakis J, Araujo H, Arce P, et al. *Geant4 – a simulation toolkit.* Nucl Instrum Methods A (2003) **506**:250. doi:10.1016/S0168-9002(03)01368-8

[9] Battiston R, Burger WJ, Calvelli V, Musenich R, Choutko V, Datskov VI, et al. *Superconductive Magnet for Radiation Shielding of Human Spacecraft*. (2011). Final Report ESTEC Contract N. 4200023087/10/NL/AF. Noordwijk.

[10] Zarana S. Patel, Tyson J. Brunstetter, William J. Tarver, Alexandra M. Whitmire, Sara R. Zwart, Scott M. Smith and Janice L. Huff *Red risks for a journey to the red planet: The highest priority human health risks for a mission to Mars* Nature PJ - Microgravity (2020) 6:33

[11] Pancotti, A., Slough, J., and Shimazu, A., *Mars Mission Trade Studies and Technology Development of a 36 MW Fusion Rocket,* Joint Conference of 30th International Symposium on Space Technology and Science, 34th International Electric Propulsion Conference, July 2015

[12] Bret G. Drake and Kevin D. Watts, *Human Exploration of Mars Design Reference Architecture 5.0 Addendum #2* NASA/SP–2009-566-ADD2

[13] A. Ballarino, R. Flükiger, *Status of MgB2 wire and cable applications in Europe* 29th International Symposium on Superconductivity, Journal of Physics: Conf. Series 871 (2017) 012098

[14] Paolo Papini, Piero Spillantini *Toroidal magnetic fields for protecting astronauts from ionizing radiation in long duration deep space missions* Acta Astronautica 104 (2014) 531–537

[15] John Slough P*lasma Magneto-Shell Aerocapture for Manned Mars Missions and Planetary Deep Space Orbiters* D4N5-TA5-S3, 47th IEEE International Conference on Plasma Science (ICOPS-2020)